iScience

CellPress
OPEN ACCESS

Article

Sustainable Design of Urban Rooftop Food-Energy-Land Nexus

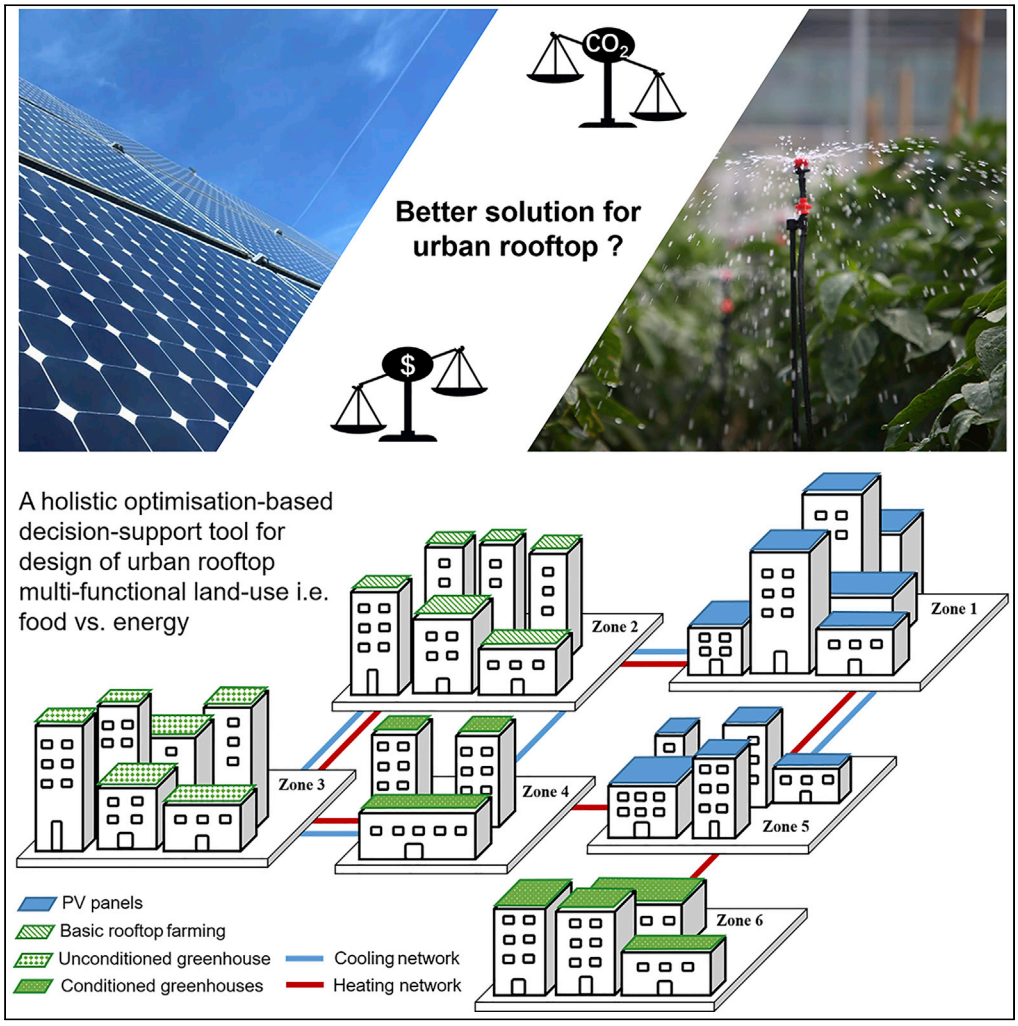

Rui Jing, Astley Hastings, Miao Guo

miao.guo@kcl.ac.uk

HIGHLIGHTS

Propose a holistic approach for optimizing urban rooftop multi-functional land-use

Biogeochemical simulations are integrated with energy system design optimization

Rooftop agriculture options can increase the flexibility of energy system design

PV is a cost-optimal option, and conditioned greenhouse offers a GHG-optimal option

Jing et al., iScience *23*, 101743
November 20, 2020
https://doi.org/10.1016/j.isci.2020.101743

iScience

CellPress
OPEN ACCESS

Article

Sustainable Design of Urban Rooftop Food-Energy-Land Nexus

Rui Jing,[1,2] Astley Hastings,[3] and Miao Guo[1,4,5,*]

SUMMARY

Urban rooftop functional design offers a promising option to enable multi-function urban land-use to deliver multiple ecosystem services, e.g., food production by rooftop agriculture and energy supply by installing photovoltaic (PV) panels. To identify the best rooftop utilization strategy considering multiple decision criteria and understand the impact of rooftop solution on the design of urban energy systems, we propose a whole system modeling framework that integrates biogeochemical simulation and multi-objective energy system optimization. We apply the framework to evaluate three rooftop agriculture options, namely, basic rooftop farming, unconditioned greenhouse, and conditioned greenhouse, and one rooftop energy supply option, i.e., PV panels, for an urban energy eco-design case in Shanghai, China. Enabling rooftop agriculture options brings more flexibility to the design and operation of energy systems. PV panels provide cost-optimal solutions, whereas conditioned greenhouse potentially delivers environmentally sustainable land-use by contributing to climate regulation ecosystem services.

INTRODUCTION

Landscapes generate multiple benefits for human society and individual well-being including housing, transportation, and a wide range of ecosystem services (ES) (Mace et al., 2012; MillenniumEcosystemAssessment, 2005). These services can be broadly categorized into four categories, i.e., provisioning services, e.g., food and energy; regulating and supporting services, e.g., climate and water regulation and waste recycling; and cultural services, e.g., recreational value. Although the need to incorporate such ES into decision support at different spatial scales is increasingly recognized, their value is often overlooked in real-world land-use planning applications (Bateman et al., 2013). Over the last decade, urban ES and urban agriculture have received increasing attentions as two-thirds of the overall population is expected to be urbanized in 2050 (Cortinovis and Geneletti, 2018; Hansen et al., 2019; IEA, 2019). With rapid urbanization and the projected 50% increase of population in the twenty-first century globally (UN, 2017), food and energy demand are expected to increase 50% and 30%, respectively, between now and 2050 (EIA, 2019; Grafton et al., 2015). This will increase resource supply stress and affect land scarcity and natural ecosystems (Folberth et al., 2020). A transformation from traditional farming toward sustainable land management and urban agriculture systems is necessary where multi-functional land-use systems and urban food production sites enable sustainable food supply for the urban consumption centers (Orsini et al., 2014). However, such transformation is hindered by conflicting ES, such as climate regulation versus the food and energy provision, which compete on the limited urban land resources (Acuto et al., 2018). How this urban populace will be sustainably fed and energized is a vital focus for governments, urban planners, and academia.

Urban rooftops offer alternative resources for multi-functional land-use (e.g., housing and urban agriculture), but its potential benefits have not been well explored. Two promising solutions are proposed in this study—(1) implementing rooftop agriculture for food production and (2) installing photovoltaic (PV) panels for energy supply. Implementing rooftop agriculture has the potential to bring a range of benefits such as reducing urban heat island effect (Coccolo et al., 2018; Hossain et al., 2019), modulating microclimates (Duarte et al., 2015; Mauree et al., 2019), and mitigating atmospheric greenhouse gas emissions (GHG, e.g., CO_2) (Sanyé-Mengual et al., 2015). It can also strengthen social connections between neighborhoods (Benis et al., 2018), as well as of people with nature (Mincyte and Dobernig, 2016). The installation of PV panels can generate power and change the role of buildings from energy consumers to prosumers (Poruschi and Ambrey, 2019). In the meantime, such distributed power generation could enhance the energy

[1]Department of Chemical Engineering, Imperial College London, London, SW7 2AZ, UK

[2]Key Lab of Urban Environment and Health, Institute of Urban Environment, Chinese Academy of Sciences, Xiamen, 361021, China

[3]Institute of Biological and Environmental Sciences, University of Aberdeen, Aberdeen, AB24 3FX, UK

[4]Department of Engineering, Strand Campus, King's College London, London, WC2R 2LS, UK

[5]Lead Contact

*Correspondence: miao.guo@kcl.ac.uk

https://doi.org/10.1016/j.isci.2020.101743

security (Kakran and Chanana, 2018; Zeng et al., 2019) and increase public awareness of climate change (Benis et al., 2017). A synergetic integration of rooftop agriculture and PV offers a solution to couple land-competing food energy with other ES (e.g., carbon and water recycling) into urban landscape decision-making by optimizing multi-functional land-use.

Despite the potential multiple benefits from integrative rooftop agriculture-PV system, sustainably planning rooftop space to meet land-competing food-energy demands in the urban context requires a whole systems approach; however, the research on rooftop system design integrated with urban food-energy-land nexus remains largely unexplored. Recent research advances include the life cycle assessment of different rooftop utilization options (Corcelli et al., 2019; Goldstein et al., 2016; Sanjuan-Delmás et al., 2018), agent-based simulation and environmental evaluation of individual options (Mittal et al., 2019; Yeo and Lee, 2018; Zeng et al., 2008), and optimization-simulation integrative modeling of agricultural land-use and ES with conflicting decision criteria, e.g., economic and environmental objectives (Garcia et al., 2019; Groot et al., 2018; Kaim et al., 2018). More recent research efforts have been made to co-locate renewables (solar, wind) with agricultural production in drylands (Barron-Gafford et al., 2019; Ravi et al., 2016) and propose holistic approaches to assess energy-food-land nexus at a larger scale (Liu et al., 2018; Van Vuuren et al., 2019). Nevertheless, research on the integrative urban rooftop system in the literature is sparse. Several modeling gaps emerged from a review of state-of-the-art literature: (1) synergetic integration of rooftop agriculture and energy to meet urban land-competing ES; (2) system implications of different rooftop design options, e.g., impacts of design option on urban energy system; and (3) systems approach with multiple design criteria to inform decision-making on urban rooftop design at community or district scales. This calls for an integrated rooftop design underpinned by a whole systems approach, which considers the multi-functional land-use and demands for multiple ES (e.g., food and energy provisioning services and carbon regulation services) (Edmondson et al., 2020; Howells and Rogner, 2014; Kinnunen et al., 2020).

We aim to address the abovementioned research gaps and present a multi-objective optimization framework to evaluate different rooftop utilization options considering the limited rooftop area. As shown in Figure 1A, a cross-disciplinary approach has been adopted in this study to bring mathematical optimization into urban planning decision-making and highlight the integration of denitrification-decomposition (DNDC) biogeochemical modeling with energy system optimization to inform rooftop planning. Specifically, we use a biogeochemical simulation to project the crop yields, inputs, and emissions of different rooftop agriculture options and further feed this information into the system design optimization model. The design optimization model optimizes the rooftop option, energy network design, energy system configuration, and operation strategy. The optimal designs are further validated by sensitivity analysis considering energy price volatility. Different objective functions lead to a set of optimal designs, and one trade-off optimal design is selected by the decision-making procedure (more details in Transparent Methods).

Figure 1B illustrates the neighborhood-level energy system with four available rooftop options. The rooftop options are closely related to the energy system design. Installing PV panels (OPT1) generates green electricity to reduce the reliance on grid electricity supply, whereas implementing rooftop agriculture options (OPT2∼OPT4) has the potential to deliver economic benefits, mitigate carbon emissions, and reduce buildings energy demands. Hence, both rooftop energy and agriculture options have the potential to contribute positively to the energy system in terms of economic and environmental footprints. A case study in Shanghai, China, demonstrates the applicability of the framework and provides insights into the optimal rooftop utilization to deliver multiple ES (i.e., food and energy provisioning). In the Results section, we have briefly described the case specifications and then analyzed the biogeochemical simulation results. This is followed by the energy system optimization modeling and detailed analyses of the optimal energy system design. We have then analyzed the impacts of different rooftop options on energy system design and presented sensitivity analyses results. The Results section is followed by Discussion, Conclusion, and Limitations of the Study sections. Related modeling details are presented in the Transparent Methods section.

RESULTS

Case Study Specifications

An urban neighborhood with 30 large commercial buildings in Shanghai, China, (Figure 2A) is used as a case study to demonstrate the model functionality, where the project lifespan is assumed as 20 years.

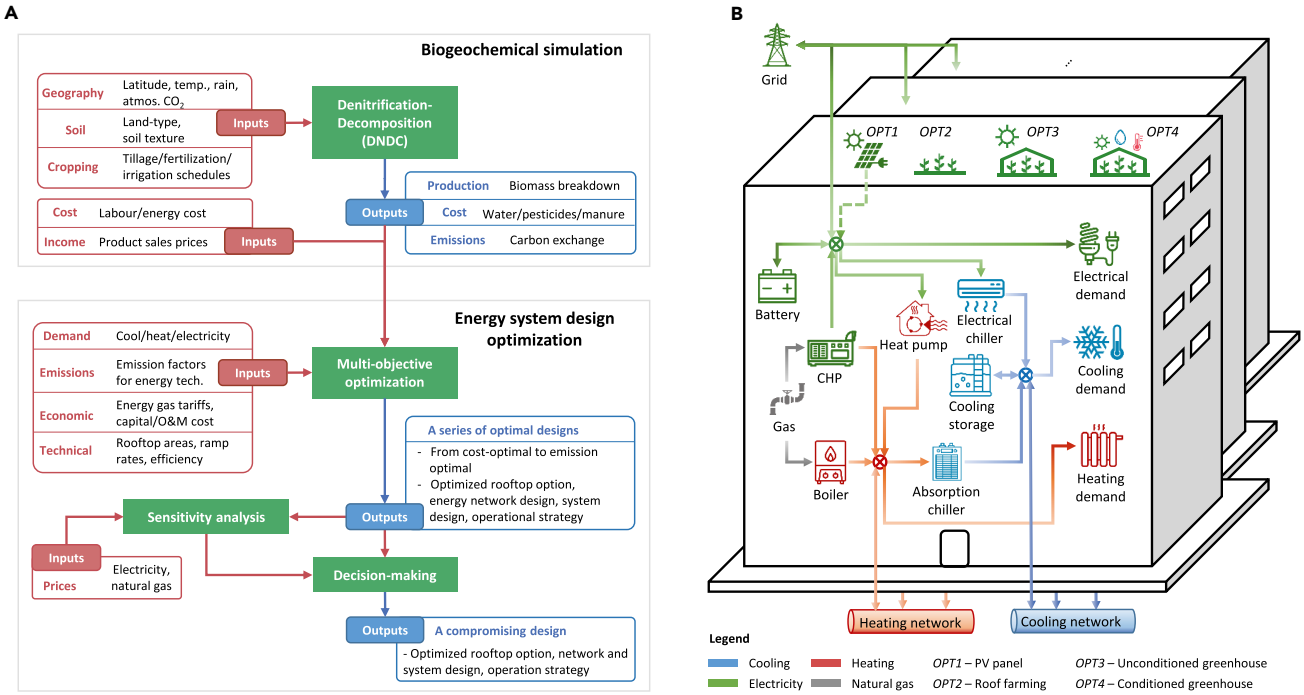

Figure 1. Overview of Integrated Modeling Framework and Illustration of the Energy Hub with Four Available Rooftop Options

(A) The proposed tool consists of two modules, i.e., biogeochemical module and energy system module. The biogeochemical module simulates the yields, inputs, and emissions of three rooftop agriculture options. This information is fed to the energy system module, by which the optimal results including the best rooftop option, energy network design, energy system configuration, and system operation strategy can be obtained.

(B) The electricity, cooling, and heating demands of all buildings within one zone are served by an energy hub. The energy hub model is generalized, including six commonly used energy supply technologies, two energy storage technologies, the interactions to the grid, as well as energy network availability (Jing et al., 2019a). On the rooftop of each building, four options are available assuming the bearing capacity of rooftop is sufficient. The optimization results will determine the best choice of the rooftop option as well as the optimal energy system configurations and hourly operational strategies.

Time-of-use electricity tariff and gas price (see Supplemental Information Figure S3) are obtained from representative data of the local market (Zhang et al., 2019). Each year is divided into three periods, namely, summer, winter, and transition period. Cooling is supplied in summer, heating is supplied in winter, and no heating or cooling demand is there in the transition period (see Supplemental Information Figure S5). A typical day is modeled for each period, and it is equally split into hourly intervals with varying solar conditions (see Supplemental Information Figure S4). All buildings are clustered into six zones (Figure 2B); the urban energy system needs to be designed optimally to simultaneously fulfill the energy demands of all zones including electricity, cooling, and heating. Within each zone, one energy hub, located at the node with the largest energy demand, can be installed to supply the energy demand of that zone via an optimally designed energy network. Energy can be transmitted between energy hubs if necessary. The shortest length of the network and guaranteed connection of all buildings is achieved in each zone by the minimum spanning tree technique (Unternährer et al., 2017). All energy hubs are connected to the utility grids as well. Four options are available for designing rooftop utilization strategies in each zone.

Figure 3 visualizes the definitions of four available rooftop options, which are closely related to the energy hub design. Installing PV panels (OPT1) can generate green electricity to reduce the reliance on grid electrical energy. In contrast, implementing rooftop agriculture options (OPT2∼OPT4) is expected to bring additional economic benefits, mitigate carbon emissions, and reduce buildings' cooling and heating demands. Hence, both rooftop energy and agriculture options have the potential to contribute positively to energy hubs in terms of economic and environmental footprints.

All energy hubs are allowed to make different choices among the four available rooftop options in our modeling framework. These four available rooftop options, i.e., PV panels and rooftop tomato farming, are further defined in Table 1 and visualized in Figure 3.

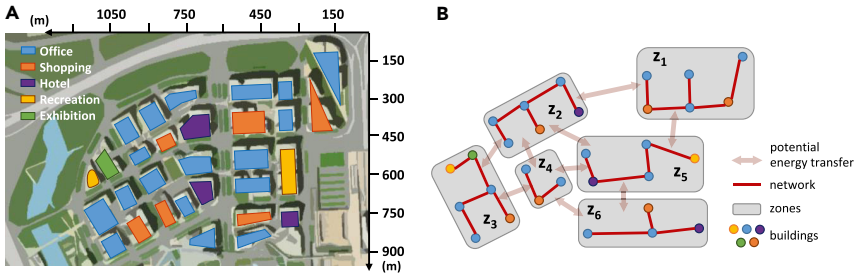

Figure 2. Basic Information of the Urban Neighborhood, Nodes (i.e., Buildings), and Network

(A) Five categories of buildings, as well as the corresponding locations and available rooftops, are plotted in Figure 2A. The available rooftop areas of each building vary between 900 and 2,500 m^2 based on the measurement from design documents as reported in Jing et al. (2019c).

(B) Each node represents one building. All nodes are classified into six clusters (i.e., zones) by k-means technique according to the locations of each building (Jing et al., 2019c).

Biogeochemical Simulation Results

We model the tomato cultivation on rooftops considering that China is one of the main tomato producers and consumers worldwide, and that tomato is rich in nutrition and acts as a key resource of daily vitamin C intake (Wikipedia, 2020). The biomass yields and C partitioning between seed, stem, leaves, and roots obtained from the DNDC model (Li et al., 1992) simulations for one crop cycle (approximately 150 days) are given in Table 2 based on daily temperature and rainfall conditions (see Supplemental Information Figure S1).

DNDC simulated the daily carbon fluxes (see Supplemental InformationFigure S2). Gross primary production (GPP) represents the total amount of carbon fixed by photosynthesis (Wang et al., 2012), whereas the net ecosystem exchange (NEE) of carbon is equivalent to the difference between GPP and ecosystem respiration (ER) (Deng et al., 2014; Elsgaard et al., 2012). ER is the biotic conversion of organic carbon to carbon dioxide by all organisms within the ecosystem (Yvon-Durocher et al., 2012), accounting for the plant respiration by root, shoot, and leaf as well as the microbial heterotrophic respiration. In DNDC, the plant respiration is simulated by a daily time step considering the effects of environmental drivers such as the atmospheric temperature and nitrogen availability. Meanwhile, the microbial heterotrophic respiration is calculated by simulating soil organic carbon decomposition (Deng et al., 2014). As shown in Table 2, DNDC projected negative NEE for one crop cycle, which indicated a net uptake of CO_2 by the plant-soil ecosystem. The NEE values vary with the options—roof farming, unconditioned greenhouse, and conditioned greenhouse can achieve −405, −974, and −1,841 kg C/ha/year, respectively. These simulation results demonstrate the beneficial effects of elevated CO_2 level in OPT4 on net carbon sequestration by plant-soil ecosystem. By incorporating the DNDC simulation results into the multi-objective optimization, the modeling framework enables urban rooftop utilization solutions to account for the biogeochemical carbon cycling.

Multi-objective Energy System Optimal Design

By integrating DNDC simulation outputs into multi-objective optimization and techno-economic parameterization, a series of different system design and rooftop utilization strategies are derived. As plotted in Figure 4, a Pareto frontier represents the trade-off between cost optimal and GHG minimization objectives, where the system design and selection of rooftop options vary significantly. Note that the cost includes the annual operation expense and the capital expenses amortized over the assumed lifetime of the project, i.e., 20 years. To further enable the decision-makers to articulate their preference of multiple decision criteria and lead to optimal solution to address the trade-offs, we apply the Technique for Order Preference by Similarity to an Ideal Solution (TOPSIS) method to choose one trade-off solution with maximum rationality of selection (Jing et al., 2019b) (more details in Transparent Methods).

Objective function moves from cost-optimal to GHG minimization, whereas the rooftop utilization transits gradually from an OPT1-PV panel-dominated solution to OPT1∼OPT4 hybrid solutions and finally selects an OPT4-conditioned greenhouse solution. Considering economic feasibility, rooftop PV panel (OPT1) is the preferable solution for most of the zones with one zone exception where roof farming (OPT2) is selected. Along the Pareto frontier, basic rooftop farming (OPT2) and unconditioned greenhouse solution

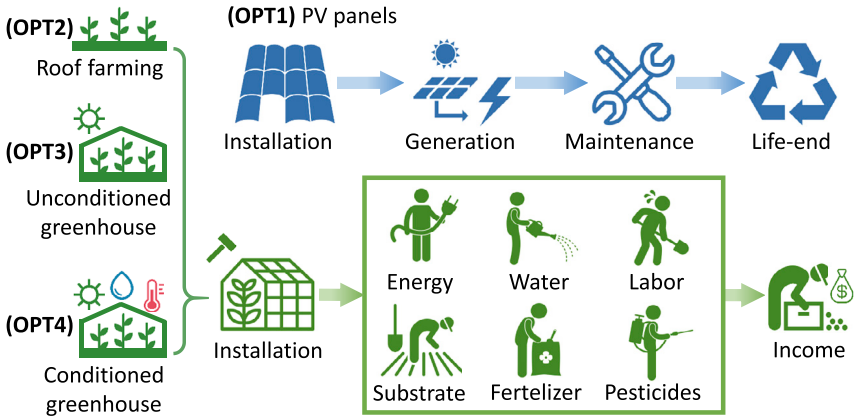

Figure 3. Definitions of Rooftop PV and Agriculture Options

For all three agriculture options, we consider the life cycle cost including installation, various processes of planting, as well as the tomato yields income. The yield, operational cost, and emission saving potential are calculated from the biogeochemical simulation. For PV option, we consider the life cycle cost, and the profit comes from generating onsite electricity. The emission saving can be achieved by using sustainable electricity instead of the grid electricity.

(OPT3) are gradually selected by most zones as the environmentally favorable choice when considering the trade-offs between economic and GHG objectives. At the emission minimization mode, all zones selected the conditioned greenhouse (OPT4) as their rooftop solution. The underlying reasons are that OPT1-PV panel tends to bring more economic benefit to the whole system compared with the other rooftop agriculture options (OPT2∼OPT4), whereas OPT2∼OPT4 could lead to more GHG reductions. Among agriculture options, OPT2-basic rooftop farming offers economically competitive option (close to OPT1-PV panel). OPT4 delivers superior GHG reduction effects despite the relatively high costs.

In the meantime, combined rooftop agriculture options (OPT2∼OPT4) could significantly increase the flexibility of energy system design. As shown in Figure 4, when only OPT4 is selected, the system performance varies within a relatively narrow range (14,200–15,200×10^3 USD/year for cost and 135–200 × 10^3 kg/year carbon emission) by just changing the energy system design. While different rooftop agriculture (OPT2∼OPT4) and energy options (OPT1) are available, the system design flexibility significantly improved with the cost and GHG objectives varying within a wider range of 13,400–15,200×10^3 USD/year and 135–445 × 10^3 kg/year, respectively.

Impact of Rooftop Options on Energy System Design

The rooftop options, as well as heating and cooling network design, for three representative solutions are visualized in Figure 5, which is consistent with the observation in Figure 4. No obvious trends can be concluded in terms of cooling and heating network design from three representative optimal solutions on the Pareto frontier. A further investigation for system implications of rooftop solutions on the energy system configuration and network design is illustrated in Figure 6.

In Figure 6, the technology sizing choices are expressed as a function of the objectives switching from cost-optimal to CO_2 emission-optimal. Several observations are summarized below.

1. With the objective moving from cost-optimal to GHG-optimal, the installed capacity of combined heating and power (CHP) and boiler dropped gradually as shown in Figures 6A and 6B. This can be partially explained by the natural gas-based technologies (CHP and boiler) offering cost-competitive design options but embedding higher CO_2 emissions. To achieve lower emission designs gradually, the installed capacities of CHP and boiler have to decrease. Consequently, less residual heat is available for absorption chiller to generate cooling; a reduced installation capacity was also observed in Figure 6E. Meanwhile, PV panel (OPT1) gives its place to agriculture options (OPT2∼OPT4) to fulfill the gradually higher requirement of the GHG objective.
2. As less capacity of the absorption chiller is installed, a larger capacity of the electric chiller is required to fulfill the cooling demand. With the increase in electric chiller capacity, more electricity is required.

Index	Option	Note
OPT1	PV panels	Install PV panels and generate sustainable electricity
OPT2	Basic rooftop farming of tomato	Basic agriculture cultivation system configuration without greenhouse or optimal control of temperature, lighting, and humidity
OPT3	Unconditioned greenhouse of tomato	Steel greenhouse structures with a plastic film cover but without temperature, lighting, and humidity control
OPT4	Conditioned greenhouse of tomato	Advanced greenhouse systems with well-configured temperature, lighting, and humidity control

Table 1. Definition of Available Rooftop Options

Due to the lower capacity of CHP, more electricity has to be imported from the grid with a higher import/export ratio as shown in Figure 6H.

3. The size of the cooling storage tank decreases followed by a rapid increase at the compromising point. Meanwhile, no obvious trends are found in cooling and heating network design; the cooling storage tank seems not to play signification role in the network design.
4. The variation degree for the capacity of each technology is different before and after the compromising point. From cost-optimal to trade-off solution, selecting different rooftop solutions (OPT1∼OPT4) produces more impacts on system design than the energy technologies themselves. By selecting different agriculture solutions (OPT2∼OPT4), CO_2 emission can be reduced efficiently. Consequently, the change of installed capacities for energy technologies is relatively moderate. Once the optimal solution passes the compromising point, the rooftop solution is constant (all select OPT4–conditioned greenhouse), whereas capacities of energy technologies vary to further reduce CO_2 emissions.

Overall, constrained by limited land resources particularly in urban areas, rooftop offers alternative options for multi-functional land-use. As presented in this study, by integrating agriculture and energy systems with urban rooftops, the land not only delivers housing benefits for human society but also has the potential to bring multiple ES (energy and food provisioning and climate regulation ES). Different rooftop options (OPT1∼OPT4) impact the ES benefits (income and climate regulation) significantly. Energy provisioning option (OPT1) brings the highest income achieving the cost-optimal rooftop land-use solution. Agriculture options (OPT2∼OPT4) bring more climate regulation ES benefits than OPT1, among which OPT4 with elevated CO_2 concentration is shown as a favorable choice to achieve a GHG minimization solution.

Sensitivity Analysis

Sensitivity analyses were carried out to understand the system implications of the electricity and natural gas prices. As demonstrated in Figures 7A and 7B, the prices of the grid electricity and the natural gas significantly impact the trade-offs between cost and emissions performances. Generally, with the increase in energy price (electricity and natural gas), the whole system costs increase. Despite the variation in prices, all scenarios achieved similar GHG performances. For each scenario, moving toward the minimal cost, the emission level increases with a reduction in energy prices. This can be explained by the higher quantity of grid electricity purchased, which offers cost-efficient energy but induces higher GHG emissions compared with onsite power generation.

Index	Option	NEE (kg C/ha/year)	Biomass Yield (kg C/ha/year)			
			Seed	Stem	Leaves	Roots
OPT-2	Basic rooftop farming	−405	170	104	104	95
OPT-3	Unconditioned greenhouse	−974	405	248	248	225
OPT-4	Conditioned greenhouse	−1,841	745	455	455	414

Table 2. DNDC Simulated Biomass Yields for Different Rooftop Agriculture Options

Figure 7C illustrates rooftop solutions along the Pareto frontier for each scenario. Although the system performances vary with energy prices, the rooftop use strategies remain relatively stable. This can explain the Pareto frontiers in Figures 7A and 7B, which are relatively evenly distributed. Overall, sensitivity analysis suggests a constant optimal solution for rooftop utilization, regardless of the energy prices variation, where PV panels (OPT1) are selected as a cost-optimal option and conditioned greenhouse (OPT4) is selected by all rooftop design to achieve minimized GHG scores.

DISCUSSION

To achieve food-energy-land nexus sustainability in an urban context, rooftop agriculture and energy systems offer promising solutions through multi-functional land-use design strategies. Four design options have been explored in the current study including solar PV panels for power generation (OPT1) and rooftop agriculture systems without and with controlled greenhouse (OPT2∼OPT4). A cross-disciplinary approach has been applied to integrate biogeochemical simulation and mathematical optimization into urban energy planning decision-making framework. The developed Mixed Integer Linear Programming model enables simultaneous optimization of rooftop utilization strategies and the whole energy system design to assess the design trade-off between the minimized costs and GHGs. This essentially represents a trade-off between provisioning and regulatory ES. Our research highlights that the PV panel (OPT1) and the rooftop greenhouse with controlled CO_2 concentration, temperature, lighting, and humidity (OPT4) offer an economically competitive and environmentally sustainable choice, respectively.

The system configurations and dispatch strategies differ significantly with the consideration of multiple conflicting objectives. Our results agree with the findings from previous studies on design of urban energy systems considering energy technologies only (Jing et al., 2019b; Li et al., 2018; Terlouw et al., 2019). Moreover, we find that enabling rooftop agriculture systems offers more flexibility for energy system design when economic and GHG objectives are considered. By merely selecting different rooftop options with

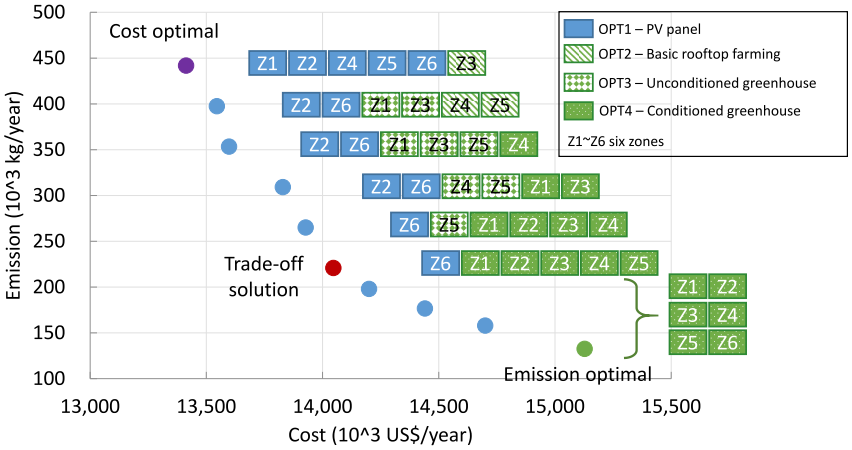

Figure 4. Pareto Frontier of Different Optimal Solutions

These solutions denote the optimal design of the whole energy system fulfilling the electricity cooling and heating demands of 30 buildings. The cost-optimal (cost-minimization), emission-optimal (CO_2-minimization), and a trade-off solution are marked by different colors.

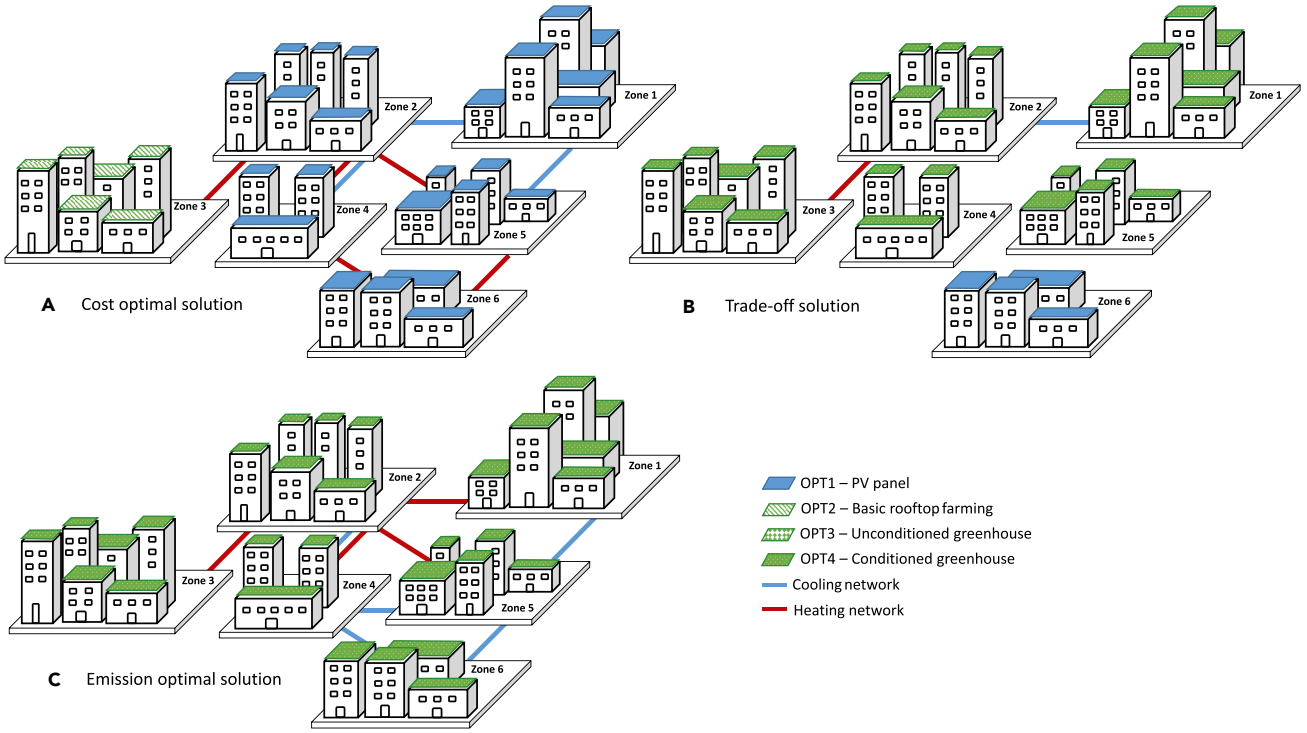

Figure 5. Optimal urban rooftop solution and corresponding energy network design with different objectives
(A–C) (A) Cost-optimal solution, (B) trade-off solution, and (C) emission-optimal solution.

a minor capacity variation of energy technologies, the GHG emission of the whole system can be reduced efficiently; once the rooftop solution is constant, the capacities of energy technologies need to vary significantly to further achieve lower emission design. Besides, earlier study has found that food production could be more beneficial than energy generation in Mediterranean climates through cost-benefit analysis of rooftop solutions only (Benis et al., 2018); however, the impact of rooftop solutions on the whole urban energy system has not been considered. The results could be case specific depending on various conditions, e.g., climate, type of buildings, food and energy prices, etc. All above observations, in turn, highlight the importance of developing tools that can bring land-competing systems (e.g., food and energy) and conflicting objectives into a whole system decision support framework to inform urban landscape design.

Notably, only carbon sequestration by the rooftop agricultural systems is accounted for in the model, where attributional carbon counting approach has been followed. However, the plants, e.g., tomato cultivated in rooftop agriculture systems can avoid the arable land-use elsewhere, which further leads to avoidance of GHG emissions caused by land-use. Thus, following a consequential carbon counting approach, the saving effects caused by land-use GHG avoidance could enhance the environmental competitiveness of rooftop agriculture systems. This study only accounts for the GHG emissions of the operation phase, which often dominates life cycle GHGs of an energy system (Wang et al., 2015). Future efforts are needed to integrate comprehensive life cycle assessment and multiple environmental impact indicators into the modeling framework.

CONCLUSION

Overall, the proposed modeling framework integrates for the first time biogeochemical simulation and multi-objective optimization to understand the implications of environmental variables (e.g., temperature, atmospheric CO_2 concentration) and crop-environment interaction on urban energy systems design. In this study, we first modeled different tomato cultivation options using biogeochemical simulation and developed a neighborhood-level energy system optimization model; the biogeochemical simulation results were fed into energy system model to resolve the bi-objective optimization to address the trade-offs between cost optimal and GHG emission minimization. An illustrative case study demonstrates the

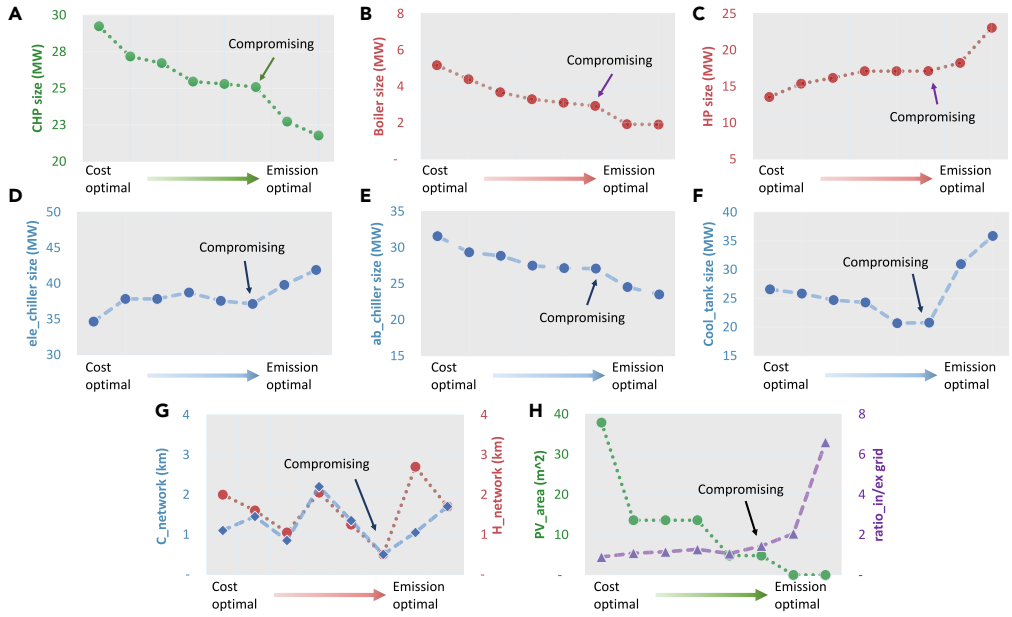

Figure 6. Size of the Installed Technologies for Different Solutions along the Pareto Frontier

(A–H) (A) CHP, (B) boiler, (C) heat pump, (D) electric chiller, (E) absorption chiller, (F) cooling storage tank, (G) cooling and heating network length, and (H) PV panel area and grid electricity import/export ratio.

applicability of the proposed decision-support tool and generates insights into the optimal design options for rooftop at a given urban neighborhood in Shanghai, China. Our research suggests that the multi-functional rooftop design from whole systems perspective enables urban food-energy-land sustainability to deliver food and energy provisioning, carbon regulation ES. The integration of agriculture options brings more flexibility to urban energy systems design when multiple conflicting objectives are considered. The PV panels provide cost-optimal rooftop solutions, whereas conditioned greenhouse potentially delivers environmentally sustainable land-use by contributing to climate regulation ES.

Limitations of the Study

This study presented a modeling framework underpinned by biogeochemical simulation and energy systems optimization to inform the rooftop utilization options. Several emerging research directions are worth further investigation efforts and highlighted below:

(1) In the current study, all building rooftops were suitable for implementing rooftop farming and PV options from building structure perspective. These building rooftops were assumed to be exposed to the sun, whereas building heights and the possible shadow effects of adjacent taller buildings were not considered. However, such effects could play significant roles in some locations, and thus are worth exploring.

(2) The urban energy model we developed is based on a green-field case when designing a new building and energy system. However, an interesting research direction would be to compare new building and building retrofit. The process of retrofitting would involve a balancing of different design elements and their effects on the overall performance (e.g., energy demand, safety) of a building; thus the design criteria, design space for building retrofit, could be significantly different from rooftop design with new building. Despite the current research on a case study in the context of China, the modeling framework developed in this study could be applied to rooftop design and case studies in other urban or hinterland areas where the building patterns and underlying parameters and design criteria would vary with the region- or country-specific climate and geographical features.

(3) The optimization modeling framework developed in this study addresses the trade-off between economic and environmental objectives and considers food/energy provisioning and climate

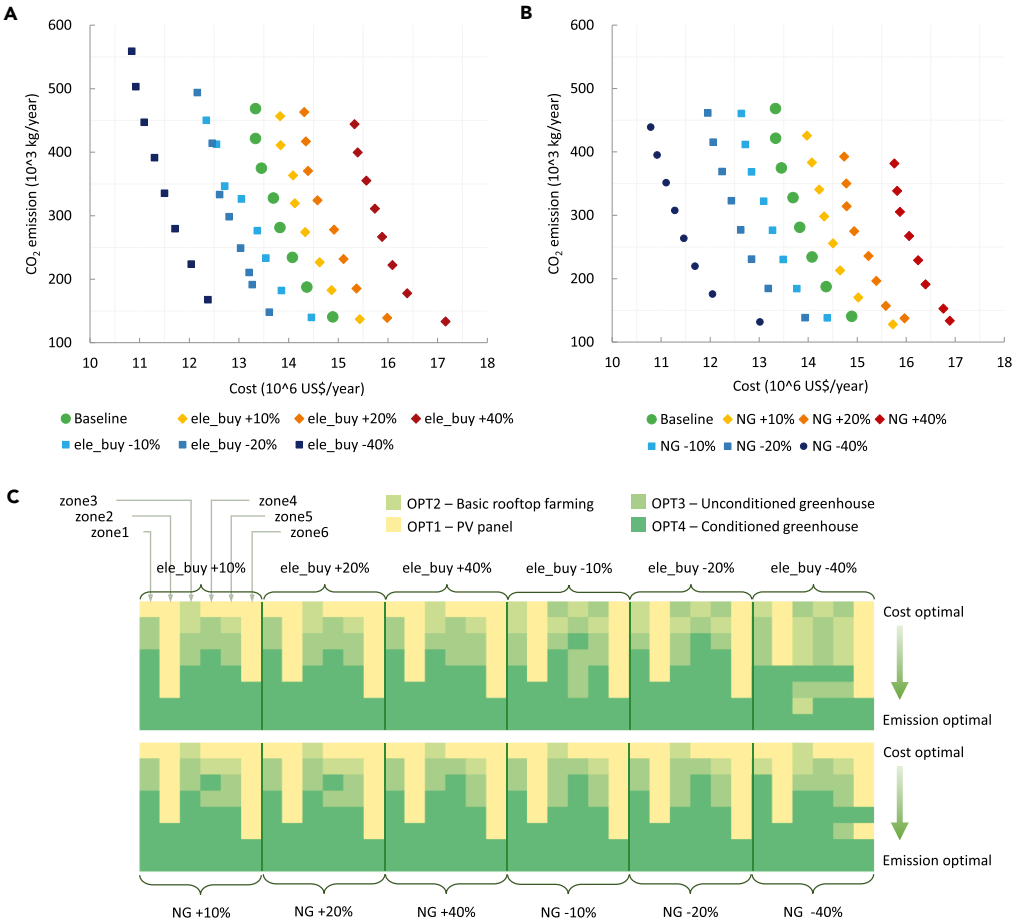

Figure 7. Electricity and Natural Gas Prices' Sensitivities on System Cost and Emissions

Assume the grid electricity price (ele_buy) and the natural gas price (NG) vary between −40% and +40% from the baseline. For both prices, six scenarios, i.e., −40%, −20%, −10%, +10%, +20%, and +40%, are evaluated.

(A) A series of Pareto frontiers led by different electricity prices.

(B) A series of Pareto frontiers led by different natural gas prices.

(C) Rooftop solutions' variations for different price-varying scenarios.

regulation ES. However, to enable such modeling framework to provide evidences for specific rooftop design solutions, inputs and feedback from multiple decision-makers (e.g., policy makers, urban planners, households) on model feasible spaces and decision criteria are important. This can be achieved by engaging multiple model users in interactive solution-searching settings to support informed decision-making. User interaction can be explored by developing a human-in-the-loop approach in multi-level modeling research to articulate the dynamic preferences of multiple decision-makers based on their gradually built understanding of the model topology and enable the solution search to be progressively directed toward the regions of interest.

(4) The current study integrated energy and agriculture system with urban rooftops to deliver housing benefits and multiple ES including energy and food provisioning and climate regulation ES. However, other potential design criteria, e.g., building safety, stability, and wider ES, e.g., water cycle-related ES, can be incorporated into the modeling framework proposed in this study and further developed in future research

(5) The current study focuses on PV and rooftop farming; however, other potential rooftop utilization strategies including renewable energy solutions, e.g., PV-wind hybrid system and recreation park, could be explored in future research investigations. The modeling framework developed in this study could be further expanded to include wider renewable energy systems in the energy system design optimization module and simulate other plant species in the biogeochemical simulation module.

(6) Another interesting future research direction is to consider urban microclimate conditions and its interaction with rooftop farming and energy systems. Either PV or vegetation on rooftops could affect the urban microclimate and consequently affect the energy performance of the urban neighborhood. For example, both rooftop PV and vegetation contribute to mitigation of the urban heat island effects and further lead to lower cooling demands as well as higher power output from PV (Berardi and Graham, 2020; Dong et al., 2020). Relevant research could be further embedded in both energy supply and demand-side of the proposed modeling framework to achieve a more holistic research.

Resource Availability

Lead Contact

Further information and requests for resources and reagents should be directed to and will be fulfilled by the Lead Contact, Miao Guo (miao.guo@kcl.ac.uk).

Materials Availability

This study did not generate new unique reagents.

Data and Code Availability

The input data are available in Supplemental Information, and the code of energy system model associated with the article is available from the Lead Contact on reasonable request.

METHODS

All methods can be found in the accompanying Transparent Methods supplemental file.

SUPPLEMENTAL INFORMATION

Supplemental Information can be found online at https://doi.org/10.1016/j.isci.2020.101743.

ACKNOWLEDGMENTS

Authors in particular M.G. would like to acknowledge the UK Engineering and Physical Sciences Research Council (EPSRC) for providing financial support for research under project "Resilient and Sustainable Bio-renewable Systems Engineering Model" [EP/N034740/1]. A.H. would like to acknowledge financial support from Natural Environment Research Council (NERC) ADVENT project [1806209].

AUTHOR CONTRIBUTIONS

R.J. and M.G. designed the study. R.J. built the integrated model and performed analyses. M.G. and A.H. contributed to the model and performed the analysis, in particular the DNDC model development and analyses. M.G. coordinated the project. All authors contributed to the manuscript.

DECLARATION OF INTERESTS

The authors declare no conflicting interests.

Received: September 21, 2020
Revised: October 17, 2020
Accepted: October 23, 2020
Published: November 20, 2020

REFERENCES

Acuto, M., Parnell, S., and Seto, K.C. (2018). Building a global urban science. Nat. Sustainability *1*, 2–4.

Barron-Gafford, G.A., Pavao-Zuckerman, M.A., Minor, R.L., Sutter, L.F., Barnett-Moreno, I., Blackett, D.T., Thompson, M., Dimond, K., Gerlak, A.K., Nabhan, G.P., et al. (2019). Agrivoltaics provide mutual benefits across the food–energy–water nexus in drylands. Nat. Sustain. *2*, 848–855.

Bateman, I.J., Harwood, A.R., Mace, G.M., Watson, R.T., Abson, D.J., Andrews, B., Binner, A., Crowe, A., Day, B.H., Dugdale, S., et al. (2013). Bringing ecosystem services into economic decision-making: land use in the United Kingdom. Science *341*, 45–50.

Benis, K., Reinhart, C., and Ferrão, P. (2017). Development of a simulation-based decision support workflow for the implementation of Building-Integrated Agriculture (BIA) in urban contexts. J. Clean. Prod. *147*, 589–602.

Benis, K., Turan, I., Reinhart, C., and Ferrão, P. (2018). Putting rooftops to use – a Cost-Benefit Analysis of food production vs. energy

generation under Mediterranean climates. Cities *78*, 166–179.

Berardi, U., and Graham, J. (2020). Investigation of the impacts of microclimate on PV energy efficiency and outdoor thermal comfort. Sustainable Cities Soc. *62*, 102402.

Coccolo, S., Kämpf, J., Mauree, D., and Scartezzini, J.-L. (2018). Cooling potential of greening in the urban environment, a step further towards practice. Sustain. Cities Soc. *38*, 543–559.

Corcelli, F., Fiorentino, G., Petit-Boix, A., Rieradevall, J., and Gabarrell, X. (2019). Transforming rooftops into productive urban spaces in the Mediterranean. An LCA comparison of agri-urban production and photovoltaic energy generation. Resour. Conserv. Recycling *144*, 321–336.

Cortinovis, C., and Geneletti, D. (2018). Ecosystem services in urban plans: what is there, and what is still needed for better decisions. Land Use Pol. *70*, 298–312.

Deng, J., Li, C., Frolking, S., Zhang, Y., Backstrand, K., and Crill, P. (2014). Assessing effects of permafrost thaw on C fluxes based on multiyear modeling across a permafrost thaw gradient at Stordalen, Sweden. Biogeosciences *11*, 4753–4770.

Dong, J., Lin, M., Zuo, J., Lin, T., Liu, J., Sun, C., and Luo, J. (2020). Quantitative study on the cooling effect of green roofs in a high-density urban Area—a case study of Xiamen, China. J. Clean. Prod. *255*, 120152.

Duarte, D.H.S., Shinzato, P., Gusson, C.d.S., and Alves, C.A. (2015). The impact of vegetation on urban microclimate to counterbalance built density in a subtropical changing climate. Urban Clim. *14*, 224–239.

Edmondson, J.L., Cunningham, H., Densley Tingley, D.O., Dobson, M.C., Grafius, D.R., Leake, J.R., McHugh, N., Nickles, J., Phoenix, G.K., Ryan, A.J., et al. (2020). The hidden potential of urban horticulture. Nat. Food *1*, 155–159.

EIA (2019). International Energy Outlook (U.S. Energy Information Administration).

Elsgaard, L., Görres, C.-M., Hoffmann, C.C., Blicher-Mathiesen, G., Schelde, K., and Petersen, S.O. (2012). Net ecosystem exchange of CO2 and carbon balance for eight temperate organic soils under agricultural management. Agric. Ecosyst. Environ. *162*, 52–67.

Folberth, C., Khabarov, N., Balkovič, J., Skalský, R., Visconti, P., Ciais, P., Janssens, I.A., Peñuelas, J., and Obersteiner, M. (2020). The global cropland-sparing potential of high-yield farming. Nat. Sustain. *3*, 281–289.

Garcia, D.J., Lovett, B.M., and You, F. (2019). Considering agricultural wastes and ecosystem services in Food-Energy-Water-Waste Nexus system design. J. Clean. Prod. *228*, 941–955.

Goldstein, B., Hauschild, M., Fernández, J., and Birkved, M. (2016). Testing the environmental performance of urban agriculture as a food supply in northern climates. J. Clean. Prod. *135*, 984–994.

Grafton, R.Q., Williams, J., and Jiang, Q. (2015). Food and water gaps to 2050: preliminary results from the global food and water system (GFWS) platform. Food Security *7*, 209–220.

Groot, J.C.J., Yalew, S.G., and Rossing, W.A.H. (2018). Exploring ecosystem services trade-offs in agricultural landscapes with a multi-objective programming approach. Landscape Urban Plann. *172*, 29–36.

Hansen, R., Olafsson, A.S., van der Jagt, A.P.N., Rall, E., and Pauleit, S. (2019). Planning multifunctional green infrastructure for compact cities: what is the state of practice? Ecol. Indic *96*, 99–110.

Hossain, M.A., Shams, S., Amin, M., Reza, M.S., and Chowdhury, T.U. (2019). Perception and barriers to implementation of intensive and extensive green roofs in dhaka, Bangladesh. Buildings *9*, 79.

Howells, M., and Rogner, H.H. (2014). Assessing integrated systems. Nat. Clim. Change *4*, 246–247.

IEA (2019). Global Status Report: Towards a Zero-Emission, Efficient and Resilient Buildings and Construction Sector (International Energy Agency).

Jing, R., Kuriyan, K., Kong, Q., Zhang, Z., Shah, N., Li, N., and Zhao, Y. (2019a). Exploring the impact space of different technologies using a portfolio constraint based approach for multi-objective optimization of integrated urban energy systems. Renew. Sustain. Energy Rev. *113*, 109249.

Jing, R., Wang, M., Zhang, Z., Liu, J., Liang, H., Meng, C., Shah, N., Li, N., and Zhao, Y. (2019b). Comparative study of posteriori decision-making methods when designing building integrated energy systems with multi-objectives. Energy Build. *194*, 123–139.

Jing, R., Wang, M., Zhang, Z., Wang, X., Li, N., Shah, N., and Zhao, Y. (2019c). Distributed or centralized? Designing district-level urban energy systems by a hierarchical approach considering demand uncertainties. Appl. Energy *252*, 113424.

Kaim, A., Cord, A.F., and Volk, M. (2018). A review of multi-criteria optimization techniques for agricultural land use allocation. Environ. Model. Softw. *105*, 79–93.

Kakran, S., and Chanana, S. (2018). Smart operations of smart grids integrated with distributed generation: a review. Renew. Sustain. Energy Rev. *81*, 524–535.

Kinnunen, P., Guillaume, J.H.A., Taka, M., D'Odorico, P., Siebert, S., Puma, M.J., Jalava, M., and Kummu, M. (2020). Local food crop production can fulfil demand for less than one-third of the population. Nat. Food *1*, 229–237.

Li, C., Frolking, S., and Frolking, T.A. (1992). A model of nitrous oxide evolution from soil driven by rainfall events: 1. Model structure and sensitivity. J. Geophys. Res. Atmos. *97*, 9759–9776.

Li, Y., Wang, J., Zhao, D., Li, G., and Chen, C. (2018). A two-stage approach for combined heat and power economic emission dispatch: combining multi-objective optimization with integrated decision making. Energy *162*, 237–254.

Liu, J., Hull, V., Godfray, H.C.J., Tilman, D., Gleick, P., Hoff, H., Pahl-Wostl, C., Xu, Z., Chung, M.G., Sun, J., et al. (2018). Nexus approaches to global sustainable development. Nat. Sustain. *1*, 466–476.

Mace, G.M., Norris, K., and Fitter, A.H. (2012). Biodiversity and ecosystem services: a multilayered relationship. Trends Ecol. Evol. *27*, 19–26.

Mauree, D., Naboni, E., Coccolo, S., Perera, A.T.D., Nik, V.M., and Scartezzini, J.-L. (2019). A review of assessment methods for the urban environment and its energy sustainability to guarantee climate adaptation of future cities. Renew. Sustain. Energy Rev. *112*, 733–746.

MillenniumEcosystemAssessment. (2005). Ecosystems and Human Well-Being: Synthesis (Island Press).

Mincyte, D., and Dobernig, K. (2016). Urban farming in the North American metropolis: rethinking work and distance in alternative food networks. Environ. Plann. A Econ. Space *48*, 1767–1786.

Mittal, A., Krejci, C.C., and Dorneich, M.C. (2019). An agent-based approach to designing residential renewable energy systems. Renew. Sustain. Energy Rev. *112*, 1008–1020.

Orsini, F., Gasperi, D., Marchetti, L., Piovene, C., Draghetti, S., Ramazzotti, S., Bazzocchi, G., and Gianquinto, G. (2014). Exploring the production capacity of rooftop gardens (RTGs) in urban agriculture: the potential impact on food and nutrition security, biodiversity and other ecosystem services in the city of Bologna. Food Secur. *6*, 781–792.

Poruschi, L., and Ambrey, C.L. (2019). Energy justice, the built environment, and solar photovoltaic (PV) energy transitions in urban Australia: a dynamic panel data analysis. Energy Res. Social Sci. *48*, 22–32.

Ravi, S., Macknick, J., Lobell, D., Field, C., Ganesan, K., Jain, R., Elchinger, M., and Stoltenberg, B. (2016). Colocation opportunities for large solar infrastructures and agriculture in drylands. Appl. Energy *165*, 383–392.

Sanjuan-Delmás, D., Llorach-Massana, P., Nadal, A., Ercilla-Montserrat, M., Muñoz, P., Montero, J.I., Josa, A., Gabarrell, X., and Rieradevall, J. (2018). Environmental assessment of an integrated rooftop greenhouse for food production in cities. J. Clean. Prod. *177*, 326–337.

Sanyé-Mengual, E., Orsini, F., Oliver-Solà, J., Rieradevall, J., Montero, J.I., and Gianquinto, G. (2015). Techniques and crops for efficient rooftop gardens in Bologna, Italy. Agron. Sustain. Dev. *35*, 1477–1488.

Terlouw, T., AlSkaif, T., Bauer, C., and van Sark, W. (2019). Multi-objective optimization of energy arbitrage in community energy storage systems using different battery technologies. Appl. Energy *239*, 356–372.

UN (2017). World Population Prospects: The 2017 Revision (Department of Economic and Social Affairs of United Nations).

Unternährer, J., Moret, S., Joost, S., and Maréchal, F. (2017). Spatial clustering for district heating integration in urban energy systems: application to geothermal energy. Appl. Energy *190*, 749–763.

Van Vuuren, D.P., Bijl, D.L., Bogaart, P., Stehfest, E., Biemans, H., Dekker, S.C., Doelman, J.C., Gernaat, D.E.H.J., and Harmsen, M. (2019). Integrated scenarios to support analysis of the food–energy–water nexus. Nat. Sustain. *2*, 1132–1141.

Wang, J., Yang, Y., Mao, T., Sui, J., and Jin, H. (2015). Life cycle assessment (LCA) optimization of solar-assisted hybrid CCHP system. Appl. Energy *146*, 38–52.

Wang, Y.P., Lu, X.J., Wright, I.J., Dai, Y.J., Rayner, P.J., and Reich, P.B. (2012). Correlations among leaf traits provide a significant constraint on the estimate of global gross primary production. Geophys. Res. Lett. *39*, 7.

Yeo, I.-A., and Lee, E. (2018). Quantitative study on environment and energy information for land use planning scenarios in eco-city planning stage. Appl. Energy *230*, 889–911.

Yvon-Durocher, G., Caffrey, J.M., Cescatti, A., Dossena, M., Giorgio, P.d., Gasol, J.M., Montoya, J.M., Pumpanen, J., Staehr, P.A., Trimmer, M., et al. (2012). Reconciling the temperature dependence of respiration across timescales and ecosystem types. Nature *487*, 472–476.

Wikipedia, 2020. Tomato (https://en.wikipedia.org/w/index.php?title=Tomato&oldid=984083723).

Zeng, J., Wu, J., Liu, J.-f., Gao, L., and Li, M. (2008). An agent-based approach to renewable energy management in eco-building. Paper presented at: 2008 IEEE International Conference on Sustainable Energy Technologies.

Zeng, X.T., Zhang, J.L., Yu, L., Zhu, J.X., Li, Z., and Tang, L. (2019). A sustainable water-food-energy plan to confront climatic and socioeconomic changes using simulation-optimization approach. Appl. Energy *236*, 743–759.

Zhang, L., Qin, Q., and Wei, Y.-M. (2019). China's distributed energy policies: evolution, instruments and recommendation. Energy Policy *125*, 55–64.

iScience, Volume *23*

Supplemental Information

Sustainable Design of Urban Rooftop Food-Energy-Land Nexus

Rui Jing, Astley Hastings, and Miao Guo

Transparent Methods

This Transparent Methods includes (1) setup and parameterisation of biogeochemical simulation, and (2) assumptions and formulations the energy system optimization model.

Biogeochemical simulation

Process-based biogeochemical model Denitrification-Decomposition tool (DNDC) is adopted in this study to simulate the plant growth and carbon and nitrogen cycles in response to environmental variables and management strategies (e.g. elevated atmospheric CO_2 concentration). The DNDC model is one of the most well-developed process-oriented biogeochemistry models and commonly utilized worldwide (Abdalla et al., 2009; Babu et al., 2006; Beheydt et al., 2007; Brown et al., 2002; Butterbach-Bahl et al., 2004; Butterbach-Bahl et al., 2001; Cai et al., 2003; Grant et al., 2004; Smith et al., 2002; Wang et al., 1997).

The DNDC model was first proposed by Li et al. (Li et al., 1992); over two-decade development, numerous changes have been implemented to DNDC model to bridge functional gaps and be adapted to region- or user-group specific versions UK-DNDC (Brown et al., 2002), DNDC-Europe (Guo et al., 2015) forest-DNDC, manure-DNDC (Li et al., 2012). A schematic family tree has been reviewed and presented by Gilhespy et al. (Gilhespy et al., 2014). A relatively complete suite of biogeochemical processes (e.g., plant growth, organic matter decomposition, fermentation, ammonia volatilization, nitrification, denitrification) has been embedded in the model, enabling computation of transport and transformations in plant-soil ecosystems. By linking with chemical engineering process design and life cycle assessment, DNDC has been applied to simulate biomass growth and carbon/nitrogen cycling in agro-ecosystems and their implications on bioproduct system sustainability (Guo et al., 2012; Guo et al., 2015). Within DNDC, the soil temperature, moisture and redox potential profiles driven by daily weather data are simulated by the soil climate sub-model considering the soil texture and plant's water demand. The crop growth and development driven by air temperature, soil water, and nitrogen supplement is simulated by the plant growth sub-model at a daily timestep. In the meantime, the decomposition sub-model tracks turnover of soil organic matters that produce CO_2 emitted from the soil as well as inorganic nitrogen released from mineralization. The other three sub-models calculate trace gas emissions from nitrification, denitrification, and fermentation, respectively. All six sub-models interact with each other to simulate the targeted ecosystem's water, C and N cycles. Overall, DNDC can predict the impacts of climate change or management alternatives on the soil biogeochemistry and the crop yield.

We use DNDC to simulate the daily tomato growth and daily net ecosystem exchange (NEE) of carbon based on the detailed parameterization and simulation setup as shown in **Table S1** in **Supplemental Information (SI)**. The 5-year (2011~2015) daily meteorological data (temperature, precipitation) for DNDC simulations were estimated based on the data obtained from the China meteorological data sharing service system (CMDC, 2018) and presented in **Fig. S1**, where the daily max-min temperature varies within a range of -5~37 ℃ and daily rainfall ranges between 0 and 25 cm.

The DNDC simulated daily NEE fluxes for one crop cycle (approximately 150 days) is presented in **Fig. S2** for different rooftop agriculture options. The annual yield and NEE (see **Table 2**) along with capital and operation cost breakdown are presented in **Table S2**. The derived income of tomato yield (calculated based on Eq. 10), the NEE, the capital and operation cost, are used to parameterize the energy system design optimization model.

Energy system design optimization

This study aims to optimize urban rooftop utilization to achieve multi-functional rooftop area use to deliver multiple ecosystem services, i.e. food and energy provisioning and climate regulation. To achieve this, we developed a multi-objective (i.e., cost and emission minimization) optimization model, which is a Mixed-Integer Linear Programming model and follows a bottom-up approach that optimizes the system design and operational strategy simultaneously. The optimization problem can be stated as follows:

Given a neighborhood of 30 buildings with known rooftop areas, locations, energy demands, weather conditions and available technology options for energy and food crop production, to ***determine*** the rooftop utilization, energy system design and operational strategy, to ***achieve*** a series of optimal system designs representing the trade-offs between two conflicting objectives i.e. the minimized annualized cost and the minimized carbon emissions. The overall electricity, cooling and heating demands of all buildings over an hourly interval time horizon must be fulfilled simultaneously, which bound the energy system design and the operational strategy. The rooftop areas and weather condition regulate the crop yields, CO_2 emissions and operational costs. The defined optimization problems investigate the cost-efficient and environmentally sustainable design and operational strategy considering capital inputs and operational configurations (e.g. energy transmission loss) and policy intervention (energy supply tariff).

Specifically, several features of the model are described below:

Energy Hub Mode. The model is developed following the energy hub mode, where 30 buildings are clustered into 6 zones by spatial clustering technique (i.e., K-means) based on the relative distances between buildings (Unternährer et al., 2017). Buildings are clustered to specific number of zones; the sum of distances between cluster centroid and buildings in that zone is minimal. Within each zone, an energy hub is assumed located at the building with the largest energy demands. The energy hub fulfils the energy demands of all buildings in that zone through an internal energy network (Perera et al., 2020), which is pre-optimized by Minimum Spanning Tree algorithm (Jing et al., 2019c). Meanwhile, each energy hub is flexible to connect to neighboring hubs if needed, depending on the optimization results. Hence, we essentially optimize the design, operation and interactions of 6 networked energy hubs along with the rooftop utilization solutions in the urban neighborhood.

Multi-objective optimization. The ε-constraint approach is applied to solve the bi-objective (i.e., cost and emissions) minimization problem. As derived in Eq. (1), the ε-constraint approach maintains the $f_1(x)$ as objective function, and converts the $f_2(x)$ to a constraint by introducing a parameter of ε. Hence, the bi-objective problem is converted to a typical single-objective problem [(Jing et al., 2019a)], $f_1(x)$ and $f_2(x)$ denote objective function of AC and ACE.

$$\begin{aligned} &\min\ f_1(x) \\ &\text{S.T.}\ \ f_2(x) \le \varepsilon \\ &\qquad \text{and other constraints from original model} \end{aligned} \tag{1}$$

By minimizing $f_1(x)$ and $f_2(x)$ individually, the minimum and maximum values of $f_2(x)$ can be obtained as $f_2^{\min}(x)$ and $f_2^{\max}(x)$. Then, for each point N+1, the value of ε can be calculated by $\varepsilon = f_2^{\max}(x) - \frac{f_2^{\max}(x) - f_2^{\min}(x)}{N}\mu$, where N is the number of self-defined intervals between minimum and maximum values of $f_2(x)$, μ=0,…,N.

Decision-making. The TOPSIS decision-making method is adopted to find one trade-off solution from a set of solutions on the Pareto frontier (Jing et al., 2019b). All solutions (i.e., points) are numbered by m in a n dimensional coordinate system in the first place. These points are then normalized and the TOPSIS method defines an ideal-point and a non-ideal point based on the distribution of the points. We further calculate the Euclidian distance (ED) of each point on the Pareto frontier to the ideal-point (ED_{m+}) and the non-ideal point (ED_{m-}), respectively, by Eq. 2(a-b). The point with relative farthest distance from the non-ideal point (i.e., biggest Y_m value) is selected as the trade-off solution (Eq. 2(c)) (Jing et al., 2018).

$$ED_{m+} = \sqrt{\sum_{n=1}(f_{m,n}^{\text{norm}} - f_n^{\text{ideal}})^2} \tag{2a}$$

$$ED_{m-} = \sqrt{\sum_{n=1}(f_{m,n}^{\text{norm}} - f_n^{\text{nadir}})^2} \tag{2b}$$

$$Y_m = \frac{ED_{m-}}{ED_{m-} + ED_{m+}} \tag{2c}$$

Sensitivity Analysis. Sensitivity analyses were conducted to validate the modelling outputs solutions considering the price variability of grid electricity and natural gas (Mavromatidis et al., 2018; Yue et al., 2018). Considering the computational time, an energy price variation range of -40% to +40% was assumed for both electricity and natural gas with an interval of every 10% fluctuation. Our optimization results suggest that the rooftop utilisation strategy is not sensitive to the energy price parameters; regardless of energy price variation, the PV panel and the conditioned greenhouse were modelled as cost-effective and GHG optimal solutions respectively.

Model Description. In the optimization model, energy demands and prices for each year, and energy conversion efficiencies (e.g. CHP efficiency) were assumed as constant. The DNDC-simulated crop yields were annualized, and the constant operational costs were assumed for plantation management (e.g. fertilization, irrigation). The key decision variables and parameters are defined in the **Table 3~Table 7** whereas the detailed parameterization is given in **Table S3**.

Table 3 Definitions of indices in the optimization model

Indices	Definitions
s	Sets of three representative seasons
h	Sets of 24 hours
i	Sets of zones
j	Sets of zones, $j \neq i$
t	Sets of energy supply devices, including PV, CHP, boiler (b), electric chiller (ec), absorption chiller (ac), heat pump (hp), battery storage (b-st), cooling storage tank (c-st)
k	Sets of three rooftop agriculture options (k=1 roof farming, k=2 unconditioned greenhouse, k=3 conditioned greenhouse)
$\overline{(\cdot)}$	Upper bound of variables

Table 4 Definitions of parameters in the optimization model

Parameters	**Definitions**
C^{CAP}	Unit capital cost [\$/kW] of CHP ($C_{\mathrm{CHP}}^{\mathrm{CAP}}$), boiler ($C_{\mathrm{b}}^{\mathrm{CAP}}$), electric chiller ($C_{\mathrm{ec}}^{\mathrm{CAP}}$),absorption chiller ($C_{\mathrm{ac}}^{\mathrm{CAP}}$), heat pump ($C_{\mathrm{hp}}^{\mathrm{CAP}}$), PV panel ($C_{\mathrm{pv}}^{\mathrm{CAP}}$) , heating and cooling network ($C_{\mathrm{pipe}}^{\mathrm{CAP}}$), battery storage ($C_{\mathrm{b\text{-}st}}^{\mathrm{CAP}}$), cooling storage tank ($C_{\mathrm{c\text{-}st}}^{\mathrm{CAP}}$); and unit capital cost [\$/m^2] of rooftop agriculture option (C_k^{CAP})
$DX_{i,j}$	Distance between zones
η	Efficiency of CHP (η^{CHP}), boiler (η^{b}), electric chiller (η^{ec}), absorption chiller (η^{ac}), heat pump (η^{hp}), PV panel ($\eta_{s,h}^{\mathrm{pv}}$), storage self-discharge ($\eta^{\mathrm{in\text{-}st}}$), storage charge/discharge ($\eta^{\mathrm{cha/disc}}$)
H-to-P	Heat-to-power rate of CHP
C_h^{NG}	Unit cost of natural gas [\$/kWh] at hour h for CHP ($C_h^{\mathrm{CHP\text{-}NG}}$), boiler ($C_h^{\mathrm{b\text{-}NG}}$)
C^{maint}	Maintenance cost [\$/kWh] of CHP ($C_{\mathrm{CHP}}^{\mathrm{maint}}$), boiler ($C_{\mathrm{b}}^{\mathrm{maint}}$), electric chiller ($C_{\mathrm{ec}}^{\mathrm{maint}}$), absorption chiller ($C_{\mathrm{ac}}^{\mathrm{maint}}$), heat pump ($C_{\mathrm{hp}}^{\mathrm{maint}}$), PV panel ($C_{\mathrm{pv}}^{\mathrm{maint}}$), battery storage ($C_{\mathrm{b\text{-}st}}^{\mathrm{maint}}$),cooling storage tank ($C_{\mathrm{c\text{-}st}}^{\mathrm{maint}}$)
CRF	Capital recovery factor for 15, 25, 30 years
C_h^{im}	unit price of grid electricity purchasing at hour h [\$/kWh]
C_h^{ex}	tariff for electricity sold back to grid at hour h [\$/kWh]
Ψ	Emission factor [kg/kWh] of the grid electricity (Ψ_{grid}) and natural gas (Ψ_{NG}); emission factor of k rooftop agriculture option (ψ_k^{agri})
A_i	Available roof area in i zones [m^2]
$\mathrm{income}_{i,k}$	annual unit income for k rooftop agriculture option in zone i [\$/m^2/year]
$\mathrm{opex}_{i,k}$	annual unit planting cost for k rooftop agriculture option in zone i [\$/m^2/year]
$\mathrm{Q}_{i,s,h}^{\mathrm{dem}}$	Demand in zone i at season s and hour h for heating ($\mathrm{Q}_{i,s,h}^{\mathrm{h\text{-}dem}}$), cooling ($\mathrm{Q}_{i,s,h}^{\mathrm{c\text{-}dem}}$)
$\mathrm{Q}_{i,s,h,k}^{\mathrm{roof}}$	Demand saved in zone i by k rooftop agriculture option for heating ($\mathrm{Q}_{i,s,h,k}^{\mathrm{h\text{-}roof}}$), cooling ($\mathrm{Q}_{i,s,h,k}^{\mathrm{c\text{-}roof}}$)
Lo^{pipe}	Thermal loss rate for cooling network ($Lo^{\mathrm{c\text{-}pipe}}$), heating network ($Lo^{\mathrm{h\text{-}pipe}}$)
$SRI_{s,h}$	Solar Radiation index at season s and hour h

M	The "big M" big enough values for M_1 and M_2

Table 5 Definitions of free variables in the optimization model

Variables	Definitions
AC	The objective of annualized cost
ACE	The objective of annualized greenhouse gas emissions

Table 6 Definitions of binary variables in the optimization model

Binary Variables	Definitions
$\varphi_{i,k}^{\text{agri}}$	=1 if select the k rooftop option in zone i
φ_{i}^{PV}	=1 if select the rooftop PV option in zone i
$\beta_{i,s,h}^{\text{CHP}}$	=1 if CHP is on for in zone i at season s hour h
$\chi_{i,s,h}^{\text{CHP}}$	=1 if CHP is switching from off to on in zone i at season s hour h
$\alpha_{i,s,h}^{\text{cha}}$	=1 if energy is charged into storage in zone i at season s hour h
$\alpha_{i,s,h}^{\text{disc}}$	=1 if energy is discharged from storage in zone i at season s hour h
$\delta_{i,s,h}^{\text{ex}}$	=1 if electricity is sold back to the grid in zone i at season s hour h
$\delta_{i,s,h}^{\text{im}}$	=1 if electricity is bought from the grid in zone i at season s hour h
$\delta_{i,j}^{\text{DH}}$	=1 if district heating network is built among zone i and j
$\delta_{i,j}^{\text{DC}}$	=1 if district cooling network is built among zone i and j
$\gamma_{i,s,h}^{\text{DH}}$	=1 if zone i is receiving heating via heating network at season s hour h
$\gamma_{i,s,h}^{\text{DC}}$	=1 if zone i is receiving cooling via cooling network at season s hour h

Table 7 Definitions of positive variables in the optimization model

Positive Variables	Definitions
$CAPEX$	The capital cost of the whole system
FC	The fuel cost
MC	The maintenance cost
GC	The grid electricity cost
FI	The food yield income
$CAP_{i,t}$	The installed capacity of energy technology t in zone i
$E_{i,s,h}^{\text{pv}}$	The electricity output from PV panel in zone i at season s hour h
$E_{i,s,h}^{\text{CHP}}$	The electricity output from CHP in zone i at season s hour h
$Q_{i,s,h}^{\text{hp}}$	The heating output from heating pump in zone i at season s hour h
$Q_{i,s,h}^{\text{b-heat}}$	The heating output from boiler in zone i at season s hour h

$Q_{i,s,h}^{\text{ac-cool}}$	The cooling output from absorption chiller in zone *i* at season *s* hour *h*
$Q_{i,s,h}^{\text{ec-cool}}$	The cooling output from electric chiller in zone *i* at season *s* hour *h*
$Q_{i,s,h}^{\text{in-st}}$	The cooling stored in storage tank in zone *i* at season *s* hour *h*
$E_{i,s,h}^{\text{in-st}}$	The electricity stored in battery in zone *i* at season *s* hour *h*
$E_{i,s,h}^{\text{im}}$	The electricity bought from the grid in zone *i* at season *s* hour *h*
$E_{i,s,h}^{\text{ex}}$	The electricity sold back to the grid in zone *i* at season *s* hour *h*
$Q_{i,j,s,h}^{\text{hf}(i,j)}$	The heating flow from zone *i* to *j* at season *s* hour *h*
$Q_{j,i,s,h}^{\text{hf}(j,i)}$	The heating flow from zone *j* to *i* at season *s* hour *h*
$Q_{i,j,s,h}^{\text{cf}(i,j)}$	The cooling flow from zone *i* to *j* at season *s* hour *h*
$Q_{j,i,s,h}^{\text{cf}(j,i)}$	The cooling flow from zone *j* to *i* at season *s* hour *h*
$Q_{i,s,h}^{\text{re-heat}}$	The heating output from CHP in zone *i* at season *s* hour *h*
$Q_{i,s,h}^{\text{cha}}$	The cooling charge into cooling storage in zone *i* at season *s* hour *h*
$Q_{i,s,h}^{\text{disc}}$	The cooling energy discharged in zone *i* at season *s* hour *h*
$E_{i,s,h}^{\text{st-in}}$	The electricity charge into battery storage in zone *i* at season *s* hour *h*
$E_{i,s,h}^{\text{st-out}}$	The electricity discharged in zone *i* at season *s* hour *h*
$NG_{i,s,h}^{\text{b}}$	The natural gas consumed by boiler in zone *i* at season *s* hour *h*
$NG_{i,s,h}^{\text{CHP}}$	The natural gas consumed by CHP in zone *i* at season *s* hour *h*

Objectives. This study considers conflicting objectives, i.e., annualized cost and GHG emissions. The annualized cost (*AC*) is calculated as Eq. (3).

$$AC = CAPEX + FC + MC + GC - FI \tag{3}$$

where *CAPEX* represents capital cost, *FC* denotes fuel cost, *MC* is maintenance cost, *GC* is the grid cost, and *FI* defines food income.

The *CAPEX* includes the capital cost of all energy device, energy network, and the potential construction of different rooftop agriculture options as shown in Eq. (4). Assuming the interest rate of 6%, the *CAPEX* is further annualized by multiplying a capital recovery factor (*CRF*) as shown in Eq. (5). The service life of energy supply devices is assumed as 20 years, 15 years for rooftop agriculture, and 30 years for the energy network considering the corresponding durability. Eq. (6) ensures at most one rooftop option selected for each zone.

$$\begin{aligned} CAPEX = & \sum_{i}\sum_{t} CAP_{i,t} \times C_{t}^{\text{CAP}} \times CRF_{t} + \sum_{i} DX_{i,j} \times C_{\text{pipe}}^{\text{CAP}} \times CRF_{\text{pipe}} \\ & + \sum_{k=1,2,3}\sum_{i} \varphi_{i,k}^{\text{agri}} \times C_{k}^{\text{CAP}} \times CRF_{\text{agri}} \quad \forall t, i, j \neq i \end{aligned} \tag{4}$$

$$CRF = \frac{\mathrm{r}\times(1+\mathrm{r})^n}{(1+\mathrm{r})^n - 1} \tag{5}$$

$$\sum_{k=1}^{3} \varphi_{i,k}^{\mathrm{agri}} + \varphi_i^{\mathrm{PV}} \le 1 \quad \forall i \tag{6}$$

where *i, j, t* denote zone number (*i* and *j*), and energy technologies (*t*), respectively. *k*=1~3 denotes three rooftop agriculture options. *CAP* indicates the installed capacity. DX represents the distance between zones. φ is a binary variable determining whether implementing one certain rooftop agriculture options or PV installations or not.

Fuel cost (*FC*) is determined by the gas consumption by all devices as derived from Eq. (7). Boiler and CHP consume gas, and the gas price for CHP is lower than boiler due to the policy incentive schemes in China favoring the distributed energy technologies (i.e., CHP).

$$FC = \sum_i \sum_s \sum_h [(\frac{E_{i,s,h}^{\mathrm{CHP}}}{\eta^{\mathrm{CHP}}} \times C_h^{\mathrm{CHP\text{-}NG}} + \frac{Q_{i,s,h}^{\mathrm{b\text{-}heat}}}{\eta^{\mathrm{b}}}) \times C_h^{\mathrm{b\text{-}NG}}] \quad \forall s,h,i \tag{7}$$

where *i s, h* denote the zones, seasons, and hours, respectively. E^{CHP} is the power generation from CHP, $Q^{\mathrm{b\text{-}heat}}$ indicates the heating supply by boiler, η is the efficiency, and C^{NG} defines the unit cost of natural gas.

Maintenance cost (*MC*) is determined by the energy output from each device and the corresponding unitary maintenance cost (C^{maint}), as displayed in Eq. (8).

$$MC = \sum_i \sum_s \sum_h (E_{i,s,h}^{\mathrm{pv/CHP}} + Q_{i,s,h}^{\mathrm{hp/b\text{-}heat}} + Q_{i,s,h}^{\mathrm{ec/ac\text{-}cool}} + Q_{i,s,h}^{\mathrm{in\text{-}st}} + E_{i,s,h}^{\mathrm{in\text{-}st}}) \times C_t^{\mathrm{maint}} \quad \forall i,s,h \tag{8}$$

where $E^{\mathrm{pv/CHP}}$ is electricity generated from PV panels and CHP, $Q^{\mathrm{ec/ac\text{-}cool}}$ represents cooling energy supply by electric chiller or absorption chiller, $E^{\mathrm{in\text{-}st}}$ and $Q^{\mathrm{in\text{-}st}}$ are cooling and electricity in storage, respectively.

Grid cost (*GC*) can be derived from Eq. (9), depending on the electricity purchasing cost and the revenue generated by the surplus electricity sold to the grid.

$$GC = C_h^{\mathrm{im}} \times \sum_i \sum_s \sum_h E_{i,s,h}^{\mathrm{im}} - C_h^{\mathrm{ex}} \times \sum_i \sum_s \sum_h E_{i,s,h}^{\mathrm{ex}} \quad \forall i,s,h \tag{9}$$

where C^{im} and C^{ex} are unit price of grid electricity purchasing and tariff for electricity sold back to grid, respectively. E^{im} and E^{ex} represent the quantity of electricity purchased and sold.

Food income (*FI*) is determined by the sales income of food produced from the rooftop agriculture system and the agriculture system operational cost (Eq. (10)).

$$FI = \sum_{i}\sum_{k} A_i \times \varphi_{i,k}^{\text{agri}} \times (\text{income}_{i,k} - \text{opex}_{i,k}) \quad \forall i,k \tag{10}$$

where A_i is the rooftop area of each zone, $\text{income}_{i,k}$ represents the annual income per unit areas (m^2) for different rooftop agriculture options, and $\text{opex}_{i,k}$ indicates the operational cost of rooftop planting.

Eq. (11) defines the annualized carbon emissions (ACE) objective.

$$ACE = \psi_{\text{NG}} \times \sum_{i}\sum_{s}\sum_{h}\left(\frac{E_{i,s,h}^{\text{CHP}}}{\eta^{\text{CHP}}} + \frac{Q_{i,s,h}^{\text{b-heat}}}{\eta^{\text{b}}}\right) + \psi_{\text{grid}} \times \sum_{i}\sum_{s}\sum_{h} E_{i,s,h}^{\text{im}} + \sum_{i}\sum_{k} \psi_{k}^{\text{agri}} \times A_i \times \varphi_{i,k}^{\text{agri}} \tag{11}$$

where Ψ_{NG}, Ψ_{grid} and Ψ^{agri} are the embedded GHG emissions of natural gas, utility grid, and different rooftop agriculture options, respectively, where negative GHGs can be induced by rooftop agriculture options due to carbon sequestration.

Constraints. The formulated MILP optimization model is subject to following equality and inequality constraints.

Three energy balances have been introduced in the MILP model, i.e., electrical, heating and cooling balance. Eq. (12) constrains the heat balance, in which the energy saving potentials ($\text{Q}^{\text{h-roof}}$) of different rooftop agriculture options due to the rooftop thermal insulation effects are modelled as user-defined parameters, which can be calculated based on the methods given in previous studies (Li and Li, 2018; Nadal et al., 2017).

$$\begin{aligned}&(\text{Q}_{i,s,h}^{\text{h-dem}} - \sum_{k=1,2,3} \varphi_{i,k}^{\text{agri}} \times \text{Q}_{i,s,h,k}^{\text{h-roof}}) + \sum_{j} Q_{i,j,s,h}^{\text{hf}(i,j)} + Q_{i,s,h}^{\text{ac-heat}} = \\ &Q_{i,s,h}^{\text{re-heat}} + Q_{i,s,h}^{\text{hp}} + Q_{i,s,h}^{\text{b-heat}} + \sum_{j} Q_{j,i,s,h}^{\text{hf}(j,i)} \times (1 - \text{Lo}^{\text{h-pipe}}) \quad \forall i,j,s,h,j \neq i\end{aligned} \tag{12}$$

where $Q^{\text{h-dem}}$ represents heating demand of one zone. φ^{agri} is binary variable determining whether a rooftop agriculture option (k) is chosen. $Q^{\text{hf}(i,j)}$ is the heating energy flow from zone i to j via network, $Q^{\text{ac-heat}}$ is the heating consumed by absorption chiller, $Q^{\text{b-heat}}$ denotes the heating generated by boiler, $Q^{\text{re-heat}}$ is the heating recovered from CHP power generation, Q^{hp} represents the heating generated by heat pump, and $Lo^{h\text{-}pipe}$ is the heat loss coefficient of the heating network.

In the cool balance, the left-hand side of Eq. (13) includes cooling demand ($Q^{\text{c-dem}}$), potential cooling demand reduction ($\text{Q}^{\text{c-roof}}$) by implementing rooftop agriculture options (φ^{agri}), cooling charge (Q^{cha}) into a cooling storage, and the cooling energy flowing from zone i to j ($Q^{\text{cf}(i,j)}$). The right-hand side items are the cooling energy supply by electrical chillers ($Q^{\text{ec-cool}}$) and absorption chillers ($Q^{\text{ac-cool}}$), the cooling energy flowing from zone j to i ($Q^{\text{cf}(j,i)}$); and the cooling energy discharged (Q^{disc}) from the storage. A cooling loss rate ($Lo^{c\text{-}pipe}$) is applied to represent the cooling transfer loss.

$$(\mathrm{Q}_{i,s,h}^{\text{c-dem}} - \sum_{k=1,2,3} \varphi_{i,k}^{\text{agri}} \times \mathrm{Q}_{i,s,h,k}^{\text{c-roof}}) + Q_{i,s,h}^{\text{cha}} + \sum_{j} Q_{i,j,s,h}^{\text{cf}(i,j)} =$$
$$Q_{i,s,h}^{\text{ac-cool}} + Q_{i,s,h}^{\text{ec-cool}} + \sum_{j} Q_{j,i,s,h}^{\text{cf}(j,i)} \times (1 - \mathrm{Lo}^{\text{c-pipe}}) + Q_{i,s,h}^{\text{disc}} \quad \forall i, j, s, h, j \neq i \tag{13}$$

Eq. (14) defines the electrical balance. The energy consumptions by electrical chiller (E^{ec}), and heat pump (E^{hp}) together with electricity sold to the grid (E^{ex}) and battery charging ($E^{\text{st-in}}$) are equivalent to the sum of the electrical power discharged from battery storage ($E^{\text{st-out}}$), energy generation by PV panels (E^{pv}), on-site CHP (E^{CHP}) and electricity purchased from grid (E^{im}).

$$E_{i,s,h}^{\text{ec}} + E_{i,s,h}^{\text{ex}} + E_{i,s,h}^{\text{hp}} + E_{i,s,h}^{\text{st-in}} + E_{i,s,h}^{\text{dem}} = E_{i,s,h}^{\text{st-out}} + E_{i,s,h}^{\text{pv}} + E_{i,s,h}^{\text{im}} + E_{i,s,h}^{\text{CHP}} \quad \forall i, s, h \tag{14}$$

In addition to the above system integration-related constraints, other physical constraints for energy systems have been modelled and presented aa follows, including capacity limits (energy outputs constrained by the installed capacities), conversion constraints (cooling/heating/electricity energy conversion), storage constraints (constraints on both battery storage and thermal storage), operation constraints (on/off and ramp-up/down control), utility grid connections, and network constraints (logical constraints on energy network design and operation) (Jing et al., 2019c).

The energy conversions are derived in Eq. 15(a ~ e).

$$Q_{i,s,h}^{\text{ec-cool}} = \eta^{\text{ec}} \times E_{i,s,h}^{\text{ec}} \quad \forall i, s, h \tag{15a}$$
$$Q_{i,s,h}^{\text{ac-cool}} = \eta^{\text{ac}} \times Q_{i,s,h}^{\text{ac-heat}} \quad \forall i, s, h \tag{15b}$$
$$Q_{i,s,h}^{\text{hp}} = \eta^{\text{hp}} \times E_{i,s,h}^{\text{hp}} \quad \forall i, s, h \tag{15c}$$
$$Q_{i,s,h}^{\text{b-heat}} = \eta^{\text{b}} \times NG_{i,s,h}^{\text{b}} \quad \forall i, s, h \tag{15d}$$
$$E_{i,s,h}^{\text{CHP}} = \eta^{\text{CHP}} \times NG_{i,s,h}^{\text{CHP}} \quad \forall i, s, h \tag{15e}$$
$$Q_{i,s,h}^{\text{re-heat}} = \text{H-to-P} \times E_{i,s,h}^{\text{CHP}} \quad \forall i, s, h$$

The power output of solar PV panels is defined at Eq. 16.

$$\eta_{s,h}^{\text{pv}} = P_1 \times [(\frac{SRI_{s,h}}{SRI_0})^{P_2} + P_3 \times (\frac{SRI_{s,h}}{SRI_0})][1 + P4 \times (\frac{T_{s,h}}{T_0})^{P_2} + P_5 \times \frac{AM_{s,h}}{AM_0}] \quad \forall s, h \tag{16a}$$
$$E_{i,s,h}^{\text{pv}} = \varphi_i^{\text{pv}} \times A_i \times \eta_{s,h}^{\text{pv}} \times SRI_{s,h} \quad \forall i, s, h \tag{16b}$$

where the efficiency of PV panel η_{pv} is related to solar radiation index (SRI) in the unit of (W/m^2), the ambient temperature (T), and the air mass (AM), SRI_0 = 1000 W/m^2, T_0 = 25℃, AM_0 = 1.5, P_1 = 0.2820, P_2 = 0.3967, P_3 = -0.4473, P_4 = -0.093, P_5 = 0.1601; A_i is the available roof area.

To keep the linearity of the model, the efficiency of each energy supply device is assumed to be constant. Consequently, specific operation constraints are applied for the CHP avoiding low part-load operations and possible efficiency drop.

The minimum part load constraint is set at 30% of full capacity to avoid CHP operating at a low load range when the engine is on.

$$E_{i,s,h}^{\text{CHP}} \leq \beta_{i,s,h}^{\text{CHP}} \times M_1 \quad \forall i, s, h \tag{17a}$$

$$E_{i,s,h}^{\mathrm{CHP}} \geq (\beta_{i,s,h}^{\mathrm{CHP}} - 1) \times M_2 + 0.3 \times CAP_i^{\mathrm{CHP}} \quad \forall i,s,h \tag{17b}$$

where CAP^{CHP} is CHP installed capacity, and β^{CHP} is a binary variable for controlling the on/off status of CHP ($\beta^{\mathrm{CHP}} = 1$ is on). In addition, M_1 and M_2 are both big enough values to achieve the linear model.

To avoid frequently on/off of CHP, only one time on/off is allowed as derived in Eq. 18.

$$\sum_h \chi_{i,s,h}^{\mathrm{CHP}} \leq 1 \quad \forall i,s,h \tag{18a}$$

$$\chi_{i,s,h}^{\mathrm{CHP}} \geq \beta_{i,s,h}^{\mathrm{CHP}} - \beta_{i,s,h-1}^{\mathrm{CHP}} \quad \forall i,s,h \tag{18b}$$

$$\chi_{i,s,h}^{\mathrm{CHP}} \leq 1 - \beta_{i,s,h-1}^{\mathrm{CHP}} \quad \forall i,s,h \tag{18c}$$

$$\chi_{i,s,h}^{\mathrm{CHP}} \leq \beta_{i,s,h}^{\mathrm{CHP}} \quad \forall i,s,h \tag{18d}$$

where χ is a binary variable controlling the maximal frequency of switching on/off.

To avoid irrational fluctuation of CHP's power output mathematically, the power output fluctuation between last and this time-step cannot be larger than 50% of CHP's installed capacity.

$$E_{i,s,h}^{\mathrm{CHP}} - E_{i,s,h-1}^{\mathrm{CHP}} \leq 0.5 \times CAP_i^{\mathrm{CHP}} \quad \forall i,s,h \tag{19a}$$

$$E_{i,s,h-1}^{\mathrm{CHP}} - E_{i,s,h}^{\mathrm{CHP}} \leq 0.5 \times CAP_i^{\mathrm{CHP}} \quad \forall i,s,h \tag{19b}$$

In this study, both battery and cooling storage are available. Due to the similarity of storage devices' constraints, Eq. 20(a ~ e) takes the cooling storage as an illustrative example. The storage balance is constrained by Eq. 20a considering energy charge (η^{cha}), discharge (η^{disc}) and in-storage ($\eta^{\text{in-st}}$) efficiency. The cooling in storage tank ($Q^{\text{in-st}}$) at each time-step should less than or equal to the installed capacity of the storage tank (CAP^{st}). In the meantime, a binary variable (α) is introduced to avoid the cooling energy charging and discharging simultaneously.

$$Q_{i,s,h}^{\text{in-st}} = \eta^{\text{in-st}} \times Q_{i,s,h-1}^{\text{in-st}} + \eta^{\mathrm{cha}} \times Q_{i,s,h}^{\mathrm{cha}} - Q_{i,s,h}^{\mathrm{disc}} / \eta^{\mathrm{disc}} \quad \forall i,s,h \tag{20a}$$

$$Q_{i,s,h}^{\text{in-st}} \leq CAP_i^{\mathrm{st}} \quad \forall i,s,h \tag{20b}$$

$$Q_{i,s,h}^{\mathrm{cha}} \leq \alpha_{i,s,h}^{\mathrm{cha}} \times \overline{Q_{i,s,h}^{\mathrm{cha}}} \quad \forall i,s,h \tag{20c}$$

$$Q_{i,s,h}^{\mathrm{disc}} \leq \alpha_{i,s,h}^{\mathrm{disc}} \times \overline{Q_{i,s,h}^{\mathrm{disc}}} \quad \forall i,s,h \tag{20d}$$

$$\alpha_{i,s,h}^{\mathrm{disc}} + \alpha_{i,s,h}^{\mathrm{cha}} \leq 1 \quad \forall i,s,h \tag{20e}$$

The power exchange between utility grid and the integrated energy system is defined by:

$$0 \leq E_{i,s,h}^{\mathrm{ex}} \leq \delta_{i,s,h}^{\mathrm{ex}} \times \overline{E_{i,s,h}^{\mathrm{ex}}} \quad \forall i,s,h \tag{21a}$$

$$0 \leq E_{i,s,h}^{\mathrm{im}} \leq \delta_{i,s,h}^{\mathrm{im}} \times \overline{E_{i,s,h}^{\mathrm{im}}} \quad \forall i,s,h \tag{21b}$$

$$\delta_{i,s,h}^{\mathrm{ex}} + \delta_{i,s,h}^{\mathrm{im}} \leq 1 \tag{21c}$$

where δ^{ex} and δ^{im} are binary variables to control the power exchange and to avoid power export and import simultaneously.

This section describes network constraints, cooling and heating network constraints are similar from the modelling perspective. The heating energy can only transfer when two zones are connected via heating pipework as defined in Eq. 22a. Moreover, the connection between two zones should less than one time as derived in Eq. 22b.

$$\sum_{j} Q^{\mathrm{hf}(i,j)}_{i,j,s,h} \le \delta^{\mathrm{DH}}_{i,j} \times \overline{Q^{\mathrm{hf}(i,j)}_{i,j,s,h}} \quad \forall i, j, s, h, j \ne i \tag{22a}$$

$$\delta^{\mathrm{DH}}_{i,j} + \delta^{\mathrm{DH}}_{j,i} \le 1 \quad \forall i, j \ne i \tag{22b}$$

where δ^{DH} is a binary variable indicating whether the connection exists or not among zones (1 is connected, 0 is not).

Similarly, cooling transfer can only happen if cooling pipework exists among zones as derived in Eq. 23.

$$\sum_{j} Q^{\mathrm{cf}(i,j)}_{i,j,s,h} \le \delta^{\mathrm{DC}}_{i,j} \times \overline{Q^{\mathrm{cf}(i,j)}_{i,j,s,h}} \quad \forall i, j, s, h, j \ne i \tag{23a}$$

$$\delta^{\mathrm{DC}}_{i,j} + \delta^{\mathrm{DC}}_{j,i} \le 1 \quad \forall i, j \ne i \tag{23b}$$

At each time step, each zone (i) cannot simultaneously receive and transfer energy to others (j) as constrained by Eq. 24.

$$\sum_{j} Q^{\mathrm{cf}(i,j)}_{i,j,s,h} \le \gamma^{\mathrm{DC}}_{i,s,h} \times \overline{Q^{\mathrm{cf}(i,j)}_{i,j,s,h}} \quad \forall i, j, s, h, j \ne i \tag{24a}$$

$$\sum_{j} Q^{\mathrm{cf}(j,i)}_{j,i,s,h} \le (1 - \gamma^{\mathrm{DC}}_{i,s,h}) \times \overline{Q^{\mathrm{cf}(j,i)}_{j,i,s,h}} \quad \forall i, j, s, h, j \ne i \tag{24b}$$

$$\sum_{j} Q^{\mathrm{hf}(i,j)}_{i,j,s,h} \le \gamma^{\mathrm{DH}}_{i,s,h} \times \overline{Q^{\mathrm{hf}(i,j)}_{i,j,s,h}} \quad \forall i, j, s, h, j \ne i \tag{24c}$$

$$\sum_{j} Q^{\mathrm{hf}(j,i)}_{j,i,s,h} \le (1 - \gamma^{\mathrm{DH}}_{i,s,h}) \times \overline{Q^{\mathrm{hf}(j,i)}_{j,i,s,h}} \quad \forall i, j, s, h, j \ne i \tag{24d}$$

where γ^{DC} is a binary variable controlling the status of transfer or receive.

The optimization model was developed in GAMS 25.0.3 and solved by the CPLEX solver on 8*12 – Core Xeon X5675 clusters with 48GB RAM. The optimality gap is set to 1%, and all other settings remain at default values.

Supplemental Reference

Abdalla, M., Wattenbach, M., Smith, P., Ambus, P., Jones, M., and Williams, M. (2009). Application of the DNDC model to predict emissions of N2O from Irish agriculture. Geoderma *151*, 327-337.

Babu, Y.J., Li, C., Frolking, S., Nayak, D.R., and Adhya, T.K. (2006). Field validation of DNDC model for methane and nitrous oxide emissions from rice-based production systems of india. Nutr Cycl Agroecosyst *74*, 157-174.

Beheydt, D., Boeckx, P., Sleutel, S., Li, C.S., and Van Cleemput, O. (2007). Validation of DNDC for 22 long-term N2O

field emission measurements. Atmos Environ *41*, 6196-6211.

Benis, K., Reinhart, C., and Ferrão, P. (2017). Development of a simulation-based decision support workflow for the implementation of Building-Integrated Agriculture (BIA) in urban contexts. Journal of Cleaner Production *147*, 589-602.

Brown, L., Syed, B., Jarvis, S.C., Sneath, R.W., Phillips, V.R., Goulding, K.W.T., and Li, C. (2002). Development and application of a mechanistic model to estimate emission of nitrous oxide from UK agriculture. Atmos Environ *36*, 917-928.

Butterbach-Bahl, K., Kesik, M., Miehle, P., Papen, H., and Li, C. (2004). Quantifying the regional source strength of N-trace gases across agricultural and forest ecosystems with process based models. Plant Soil *260*, 311-329.

Butterbach-Bahl, K., Stange, F., Papen, H., and Li, C.S. (2001). Regional inventory of nitric oxide and nitrous oxide emissions for forest soils of southeast Germany using the biogeochemical model PnET-N-DNDC. J Geophys Res-Atmos *106*, 34155-34166.

Cai, Z.C., Sawamoto, T., Li, C.S., Kang, G.D., Boonjawat, J., Mosier, A., Wassmann, R., and Tsuruta, H. (2003). Field validation of the DNDC model for greenhouse gas emissions in East Asian cropping systems. Glob Biogeochem Cycle *17*, 10.

CMDC (2018). China meteorological data sharing service system (http://data.cma.cn).

Gilhespy, S.L., Anthony, S., Cardenas, L., Chadwick, D., del Prado, A., Li, C., Misselbrook, T., Rees, R.M., Salas, W., Sanz-Cobena, A.*, et al.* (2014). First 20 years of DNDC (DeNitrification DeComposition): Model evolution. Ecological Modelling *292*, 51-62.

Grant, B., Smith, W.N., Desjardins, R., Lemke, R., and Li, C. (2004). Estimated N2O and CO2 emissions as influenced by agricultural practices in Canada. Paper presented at: 12th International Soil Conservation Organization Conference (ISCO) (Beijing, PEOPLES R CHINA: Kluwer Academic Publ).

Guo, M., Li, C., Bell, J.N.B., and Murphy, R.J. (2012). Influence of Agro-Ecosystem Modeling Approach on the Greenhouse Gas Profiles of Wheat-Derived Biopolymer Products. Environmental Science & Technology *46*, 320-330.

Guo, M., Li, C., Facciotto, G., Bergante, S., Bhatia, R., Comolli, R., Ferré, C., and Murphy, R. (2015). Bioethanol from poplar clone Imola: an environmentally viable alternative to fossil fuel? Biotechnol Biofuels *8*, 1-21.

Jing, R., Kuriyan, K., Kong, Q., Zhang, Z., Shah, N., Li, N., and Zhao, Y. (2019a). Exploring the impact space of different technologies using a portfolio constraint based approach for multi-objective optimization of integrated urban energy systems. Renewable and Sustainable Energy Reviews *113*, 109249.

Jing, R., Wang, M., Zhang, Z., Liu, J., Liang, H., Meng, C., Shah, N., Li, N., and Zhao, Y. (2019b). Comparative study of posteriori decision-making methods when designing building integrated energy systems with multi-objectives. Energy and Buildings *194*, 123-139.

Jing, R., Wang, M., Zhang, Z., Wang, X., Li, N., Shah, N., and Zhao, Y. (2019c). Distributed or centralized? Designing district-level urban energy systems by a hierarchical approach considering demand uncertainties. Applied Energy *252*, 113424.

Jing, R., Zhu, X., Zhu, Z., Wang, W., Meng, C., Shah, N., Li, N., and Zhao, Y. (2018). A multi-objective optimization and multi-criteria evaluation integrated framework for distributed energy system optimal planning. Energy Conversion and

Management *166*, 445-462.

Li, C., Frolking, S., and Frolking, T.A. (1992). A model of nitrous oxide evolution from soil driven by rainfall events: 1. Model structure and sensitivity. Journal of Geophysical Research: Atmospheres *97*, 9759-9776.

Li, C., Salas, W., Zhang, R., Krauter, C., Rotz, A., and Mitloehner, F. (2012). Manure-DNDC: a biogeochemical process model for quantifying greenhouse gas and ammonia emissions from livestock manure systems. Nutr Cycl Agroecosyst *93*, 163-200.

Li, H., and Li, X. (2018). Benchmarking energy performance for cooling in large commercial buildings. Energy and Buildings *176*, 179-193.

Liang, L., Ridoutt, B.G., Wu, W., Lal, R., Wang, L., Wang, Y., Li, C., and Zhao, G. (2019). A multi-indicator assessment of peri-urban agricultural production in Beijing, China. Ecological Indicators *97*, 350-362.

Mavromatidis, G., Orehounig, K., and Carmeliet, J. (2018). Uncertainty and global sensitivity analysis for the optimal design of distributed energy systems. Applied Energy *214*, 219-238.

Nadal, A., Llorach-Massana, P., Cuerva, E., López-Capel, E., Montero, J.I., Josa, A., Rieradevall, J., and Royapoor, M. (2017). Building-integrated rooftop greenhouses: An energy and environmental assessment in the mediterranean context. Applied Energy *187*, 338-351.

Perera, A.T.D., Nik, V.M., Chen, D., Scartezzini, J.-L., and Hong, T. (2020). Quantifying the impacts of climate change and extreme climate events on energy systems. Nature Energy.

Smith, W.N., Desjardins, R.L., Grant, B., Li, C., Lemke, R., Rochette, P., Corre, M.D., and Pennock, D. (2002). Testing the DNDC model using N2O emissions at two experimental sites in Canada. Can J Soil Sci *82*, 365-374.

Unternährer, J., Moret, S., Joost, S., and Maréchal, F. (2017). Spatial clustering for district heating integration in urban energy systems: Application to geothermal energy. Applied Energy *190*, 749-763.

Wang, Y.P., Meyer, C.P., Galbally, I.E., and Smith, C.J. (1997). Comparisons of field measurements of carbon dioxide and nitrous oxide fluxes with model simulations for a legume pasture in southeast Australia. J Geophys Res-Atmos *102*, 28013-28024.

Yue, X., Pye, S., DeCarolis, J., Li, F.G.N., Rogan, F., and Gallachóir, B.Ó. (2018). A review of approaches to uncertainty assessment in energy system optimization models. Energy Strategy Reviews *21*, 204-217.

Supplemental Figures

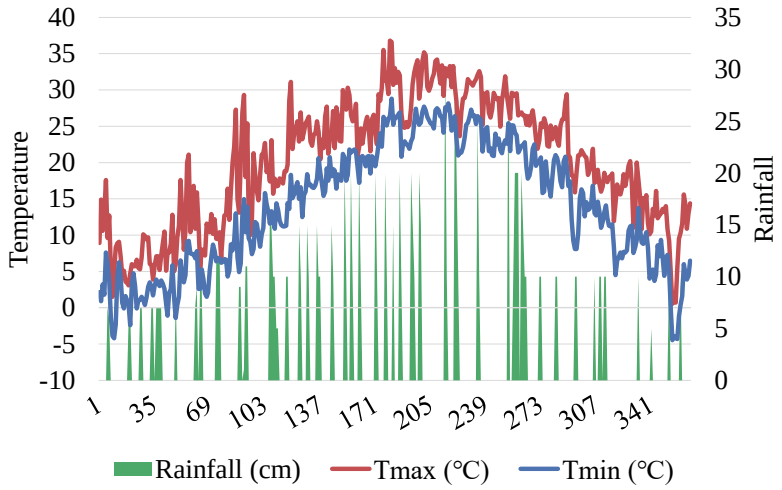

Fig S1 Daily maximum and minimum temperature and rainfall conditions for DNDC simulations, Related to Table 2. Tmax – maximum temperature (°C), Tmin – minimum temperature (°C), rainfall (cm).

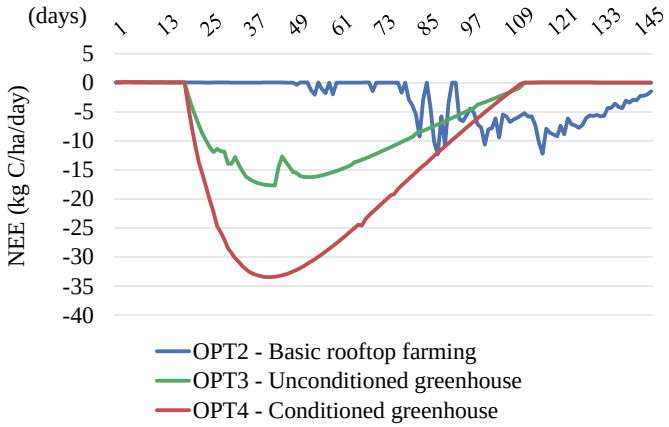

Fig S2 DNDC simulated daily NEE fluxes for one crop cycle (approximately 150 days) for different rooftop agriculture options, Related to Table 2.

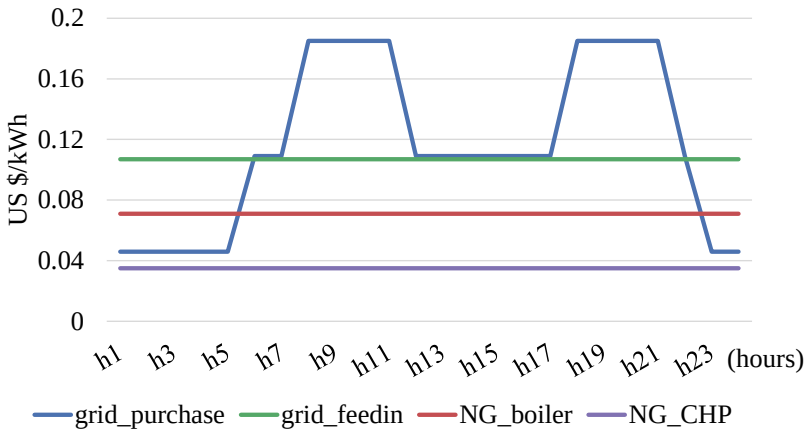

Fig S3 Different categories of time-of-use energy prices, Related to Figure 4, 5, 6, and 7. Tariffs includes the peak/non-peak electricity purchase tariff, constant electricity feed-in tariff, and different prices for CHP or boiler natural gas (NG) consumption.

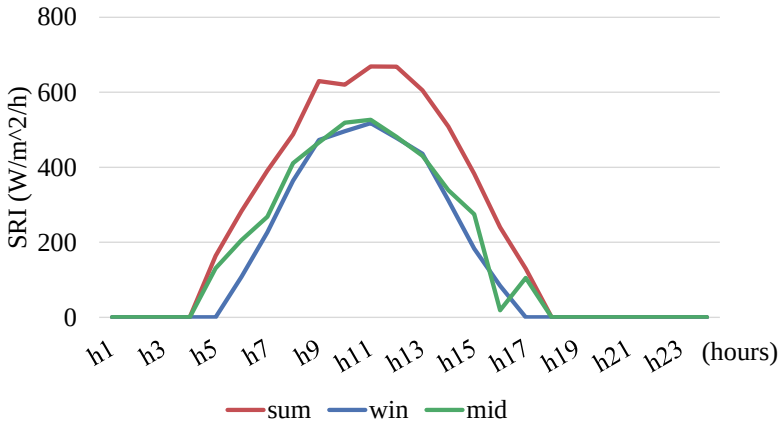

Fig S4 Solar radiation index for different seasons (sum – summer, win – winter, mid – transition), Related to Figure 4, 5, 6, and 7.

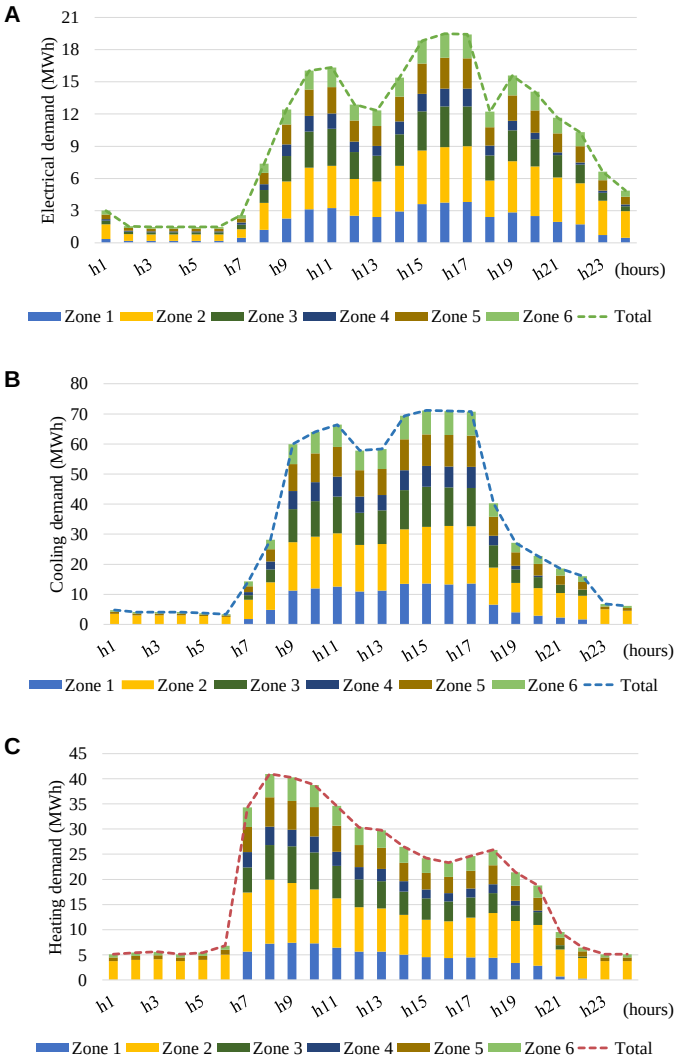

Fig S5 Hourly energy demand breakdown by zones, Related to Figure 4, 5, 6, and 7. Assuming the electricity demand for winter, summer, and transition seasons are similar as shown in Fig. S5A. The typical day cooling demand is shown in Fig. S5B, which only happens in summer. The corresponding heating demand in winter is shown in Fig. S5C.

Supplemental Tables

Table S1 Plant parameters for DNDC simulations with varying management strategies, Related to Table 2

Plant parameter	Value			Notes
	OPT2 – Basic roof farming	OPT3 – Unconditioned greenhouse	OPT4 – Conditioned greenhouse	
Maximum biomass yield	210	505	950	kg C/ha/yr
Biomass fraction	0.36/0.22/0.22/0.2	0.36/0.22/0.22/0.2	0.36/0.22/0.22/0.2	fruit/leaf/stem/root
C/N ratio	26/26/26/45	26/26/26/45	26/26/26/45	fruit/leaf/stem/root
Total N demand	205	525	929	kg N/ha/yr
Thermal degree days (TDD)	1400	1400	1400	°C
Water requirement	1300	3120	5822	kg water/kg dry matter
N fixation	1	1	1	Plant N/N taken from soil
Optimum temperature	25	25	25	°C
Fertilization	Precision	Precision	Precision	Auto applied if needed
Irrigation	Auto	Auto	Auto	Irrigation index 0.9
CO_2 concentration	350	350	500	ppm
Controlled temperature if available	NA	NA	25	°C

316 **Table S2 Cost coefficients for three rooftop agriculture options, Related to Figure 4, 5, 6, and 7 (Benis et al.,**
317 **2017; Liang et al., 2019)**

	Basic roof farming (OPT2)	Unconditioned greenhouse (OPT3)	Conditioned greenhouse (OPT4)
Capital cost ($/m^2)	15	30	45
Fertilizer ($/m^2/y)	0.06	0.60	1.10
Water ($/m^2/y)	0.42	0.31	0.48
Energy ($/m^2/y)	0.20	0.40	2.00
Substrate ($/m^2/y)	0	0.23	0.50
Labor ($/m^2/y)	2.85	4.50	8.00
Pesticides ($/m^2/y)	0	0.83	1.20
Operation total ($/m^2/y)	3.53	6.87	13.28

318

319 **Table S3 A list of parameters applied in the optimization model, Related to Figure 4, 5, 6, and 7**

Parameters	Definitions	Value
$C_{\text{CHP}}^{\text{CAP}}$	Unit capital cost of CHP [$/kW]	1,000
$C_{\text{b}}^{\text{CAP}}$	Unit capital cost of boiler [$/kW]	60
$C_{\text{ec}}^{\text{CAP}}$	Unit capital cost of electric chiller [$/kW]	120
$C_{\text{ac}}^{\text{CAP}}$	Unit capital cost of absorption chiller [$/kW]	170
$C_{\text{hp}}^{\text{CAP}}$	Unit capital cost of heat pump [$/kW]	140
$C_{\text{pv}}^{\text{CAP}}$	Unit capital cost of PV panel [$/kW]	650
$C_{\text{pipe}}^{\text{CAP}}$	Unit capital cost of heating and cooling network [$/m]	200
$C_{\text{b-st}}^{\text{CAP}}$	Unit capital cost of battery storage [$/kWh]	2,000
$C_{\text{c-st}}^{\text{CAP}}$	Unit capital cost of cooling storage tank [$/kWh]	35
C_{k}^{CAP}	Unit capital cost of k rooftop agriculture option [$/m^2]	See Table S3
$DX_{i,j}$	Distance between zones	See Fig. 2A
η^{CHP}	Efficiency of CHP (ele)	0.4
H-to-P	Heat-to-power rate of CHP	0.75
η^{b}	Efficiency of boiler	0.85
η^{ec}	Efficiency of electric chiller	4
η^{ac}	Efficiency of absorption chiller	1.2
η^{hp}	Efficiency of heat pump	2.5
η^{pv}	Efficiency of PV panel	0.14
$\eta^{\text{in-st}}$	Efficient of cooling storage self-discharge	0.9
$\eta^{\text{cha/disc}}$	Efficient of cooling storage charge/discharge	0.9
$C_{h}^{\text{CHP-NG}}$	Unit cost of natural gas for CHP [$/kWh]	See Fig. S3
$C_{h}^{\text{b-NG}}$	Unit cost of natural gas for boiler [$/kWh]	See Fig. S3
$C_{\text{CHP}}^{\text{maint}}$	Maintenance cost of CHP [$/kWh]	0.003

$C_{\mathrm{b}}^{\mathrm{maint}}$	Maintenance cost of boiler [$/kWh]	0.0003
$C_{\mathrm{ec}}^{\mathrm{maint}}$	Maintenance cost of electric chiller [$/kWh]	0.001
$C_{\mathrm{ac}}^{\mathrm{maint}}$	Maintenance cost of absorption chiller [$/kWh]	0.001
$C_{\mathrm{hp}}^{\mathrm{maint}}$	Maintenance cost of heat pump [$/kWh]	0.001
$C_{\mathrm{pv}}^{\mathrm{maint}}$	Maintenance cost of PV panel [$/kWh]	0.003
$C_{\mathrm{b\text{-}st}}^{\mathrm{maint}}$	Maintenance cost of battery storage [$/kWh]	0.003
$C_{\mathrm{c\text{-}st}}^{\mathrm{maint}}$	Maintenance cost of cooling storage tank [$/kWh]	0.0003
CRF	Capital recovery factor for 15, 25, 30 years	0.103, 0.085, 0.073
C_h^{im}	unit price of grid electricity purchasing at hour h [$/kWh]	See Fig. S3
C_h^{ex}	tariff for electricity sold back to grid at hour h [$/kWh]	See Fig. S3
Ψ_{grid}	Emission factor of the grid electricity [kg/kWh]	0.55
Ψ_{NG}	Emission factor of natural gas power generation [kg/kWh]	0.18
ψ_k^{agri}	Emission factor of k rooftop agriculture option	See Table 2
A_i	Available roof area in i zones [m^2]	900~2,500
$\mathrm{income}_{i,k}$	Income for k rooftop agriculture option in zone i [$/$m^2$/year]	3.71, 8.87, 16.26
$\mathrm{Q}_{i,s,h}^{\mathrm{h\text{-}dem}}$	Heating demand in zone i at season s and hour h	See Fig. S5
$\mathrm{Q}_{i,s,h}^{\mathrm{c\text{-}dem}}$	Cooling demand in zone i at season s and hour h	See Fig. S5
$\mathrm{Q}_{i,s,h,k}^{\mathrm{h\text{-}roof}}$	Heating demand saved in zone i by k rooftop agriculture option	4%, 5%, 6% of the original demand
$\mathrm{Q}_{i,s,h,k}^{\mathrm{c\text{-}roof}}$	Cooling demand saved in zone i by k rooftop agriculture options	4%, 5%, 6% of the original demand
$Lo^{\mathrm{c\text{-}pipe}}$	Cooling network thermal loss rate	6%
$Lo^{\mathrm{h\text{-}pipe}}$	Heating network thermal loss rate	5%
$SRI_{s,h}$	Solar Radiation index at season s and hour h	See Fig. S4

320